Solvothermal synthesis of mesoporous TiO2 with tunable surface area, crystal size and surface hydroxylation for efficient photocatalytic acetaldehyde degradation

Solvothermal synthesis of mesoporous TiO_2 with tunable surface area, crystal size and surface hydroxylation for efficient photocatalytic acetaldehyde degradation

Kaimin Zhang[a,*], Jinxin Wang[a,b], Rajeshreddy Ninakanti[c,d,e], Sammy W. Verbruggen[c,d,*]

[a]Laboratory for Adsorption and Catalysis (LADCA), Department of chemistry, University of Antwerp, Universiteitsplein 1, 2610, Wilrijk, Belgium

[b]Plasma Lab for Applications in Sustainability and Medicine - ANTwerp, Department of Chemistry, University of Antwerp, Universiteitsplein 1, 2610 Wilrijk, Antwerp, Belgium

[c]Sustainable Energy, Air & Water Technology (DuEL), Department of Bioscience Engineering, University of Antwerp, Groenenborgerlaan 171, 2020, Antwerp, Belgium

[d]NANOlab Center of Excellence, Groenenborgerlaan 171, 2020 Antwerp, Belgium

[e]Electron Microscopy for Material Science (EMAT), Department of Physics, University of Antwerp, Groenenborgerlaan 171, 2020 Antwerp, Belgium

*Corresponding author: kaimin.zhang@uantwerpen.be, sammy.verbruggen@uantwerpen.be.

Abstract

Photocatalytic acetaldehyde degradation exhibits satisfactory performance only at relatively low acetaldehyde flow rates, predominately below 10×10^{-3} mL/min, leaving ample room for improvement. Therefore, it is necessary to prepare more efficient photocatalysts for acetaldehyde degradation. Moreover, the impact of the interaction strength between the titania surface and surface water on the photocatalytic acetaldehyde efficiency is poorly understood. To address these issues, in this work a series of (001)-faceted anatase titania samples with various surface properties and structures were synthesized via a solvothermal method and tested at high acetaldehyde flow rates under UV light irradiation. With increasing solvothermal time, the pore volume, surface area, and the abundance of surface OH groups all increased, while the crystallite size decreased. These were all identified to be beneficial to promote the degradation performance. When the solvothermal temperature was 180 °C and the reaction

time was 5 h, the prepared sample displayed the most efficient performance at 19.25× 10^{-3} mL/min of acetaldehyde (conversion of (74 ± 1)% *versus* (29 ± 1)% for P25), and achieved a 100 % conversion at 16 × 10^{-3} mL/min. A weaker interaction strength between surface water and the titania surface was found to improve the acetaldehyde adsorption capacity, thereby promoting the acetaldehyde degradation efficiency. The stability of the best performing sample was tested over 48 h, demonstrating a highly stable performance with no signs of deactivation. Even at a relative humidity of 30 %, the acetaldehyde conversion retains 82% of its efficiency in a dry atmosphere, highlighting its potential in practical applications.

Keywords: surface water; mesoporous structures; nanocrystals; (001) facets; acetaldehyde; photocatalysis

1. Introduction

Volatile organic compounds (VOCs), which can be found both indoors and outdoors, constitute an important class of air pollutants that affect human health [1]. For instance, acetaldehyde is a prevalent component of indoor VOCs, originating from building materials (e.g. glues for furniture), incomplete combustion from fireplaces and biological activity of human beings [2–4]. VOCs are known to cause 'sick building syndrome' when people are exposure to this kind of environment for a prolonged period of time, ultimately even reducing life expectancy [2]. It is therefore crucial to address this problem and develop technologies to improve air quality.

To capture VOCs from the air, several recovery techniques have been proposed, such as absorption [5], adsorption [6], condensation [7], amongst others. These techniques typically involve collecting VOCs for subsequent post-treatment, allowing control of the amount of VOCs in a certain range. However, VOCs are not destroyed by these recovery methods. In contrast, destruction techniques such as thermal oxidation and photocatalytic oxidation (PCO) are more beneficial, given the direct degradation of VOCs, oxidizing hydrocarbons into CO_2

and H_2O [8,9]. However, conventional thermal oxidation is not economically feasible for air purification when the pollutants are present at low concentrations, as it permanently requires temperatures ranging from 200 °C to 1200 °C for efficient operation, causing relatively high operational costs [9]. As compared to that, photocatalytic degradation of VOCs can be induced by sunlight or room light, during which photogenerated electrons and holes combine with oxygen and/or water to produce reactive radicals, capable of fully mineralizing acetaldehyde into CO_2 and water. This method provides potential advantages such as room-temperature feasibility, ease of use, economic viability, and sustainability [8,10–13]. Titania (TiO_2), due to its relatively high photocatalytic activity, cost-effectiveness and chemical stability [14], shows potential in various photocatalytic application fields, including the decomposition of VOCs and soot [10,15,16], as well as the reduction of carbon dioxide [17] and nitrous oxide [18,19], amongst others.

However, the photocatalytic degradation of VOCs using TiO_2 is still not sufficiently mature, with limited real-life applications, and ample room for the improvement in terms of VOCs degradation performance. Therefore, researchers have attempted to enhance the performance through improvements in both the preparation of photocatalysts and the design of reactors [13,20,21]. The fabrication of photocatalysts requires considering various structures and physico-chemical properties to improve the photocatalytic efficiency [22–26]. A porous structure and high surface area are the main driving forces to achieve a higher photocatalytic performance in the degradation of gaseous VOCs. This is due to the decreased mass transfer resistance, increased exposure of surface active sites, and enhanced accessibility for gas molecules [22,27,28]. Although the porous structure and high surface area of TiO_2 can be achieved by hybridizing it with materials possessing these properties, such as silica or zeolites, the photocatalytic performance still depends on the content and properties of the photoactive TiO_2 phase. Given this, the preparation of pure porous TiO_2 materials with a high surface area,

which have the highest content of TiO_2, is an interesting solution that holds great promise for the photocatalytic degradation of acetaldehyde. G. He *et al*. synthesized mesoporous TiO_2 nanotubes with a high surface area of 78.4 m^2/g via a dual-template method, reaching an acetaldehyde conversion of up to 92 % [29]. However, the flow rate of acetaldehyde employed was relatively low, only 40 ppm at a total flow rate of 100 mL/min. Therefore, the photocatalytic performance of acetaldehyde degradation is still limited. Moreover, surface interaction sites (OH groups) and surface water on the surface of TiO_2 also play a vital role in photocatalytic acetaldehyde degradation. Hydroxyl groups provide interaction sites for the adsorption of acetaldehyde (and intermediates) [30]. However, a high content of OH groups renders the TiO_2 surface too hydrophilic, which might lead to the adsorption of excessive water. Whereas acetaldehyde is soluble in water, it is still in competition for adsorption sites with surface-bound water. Consequently, the photocatalytic acetaldehyde degradation is impeded as well. G. Zhang *et al.* and B.I. Stefanov *et al*. investigated the effect of relative humidity on VOCs (acetaldehyde, acetone, p-xylene) degradation performance of TiO_2 [31,32]. They found water indeed competed with VOCs to adsorb on the TiO_2 surface, leading to a decreased degradation performance. In the reported studies, researchers have extensively investigated the effect of water content on VOC degradation efficiency by adjusting the humidity during the photocatalytic process [31,33,34]. K. Demeestere *et al*. reported that the affinity between the TiO_2 surface and organic compounds was different with changes in water content [34]. However, the impact of interaction strength between surface water and the TiO_2 surface on photocatalytic VOC degradation has not been studied in detail. For gas-solid photocatalysis, it is meaningful and essential to investigate this surface interaction strength, providing a deeper understanding of the photocatalytic process.

In addition, it is found that acetaldehyde exhibits a higher adsorption affinity towards anatase TiO_2 compared to rutile TiO_2, resulting in a degradation efficiency five times higher than that

of rutile [35]. The acetaldehyde degradation could be further improved by creating small-sized nanocrystalline anatase [31,36,37]. Zhang *et al.* investigated the influence of calcination temperature in preparing TiO_2/diatomite composites on VOCs (formaldehyde, acetone and p-xylene) photocatalytic degradation [31]. They found that the small anatase TiO_2 crystallite size and high surface area were mainly responsible for the enhanced performance. Moreover, the existence of (001) facets on anatase TiO_2 is another beneficial parameter in promoting VOCs degradation, due to their more reactive features than thermodynamically stable (101) facets [38,39]. B.I. Stefanov *et al.* prepared anatase TiO_2 films with preferably exposed (001) facets [32]. They found that the films were more tolerant to changes in humidity than films with a random orientation.

Based on the aforementioned findings, this study has the following goals. Firstly, mesoporous anatase TiO_2 is synthesized with high surface area, composed of preferentially exposed (001) facets and small crystallite sizes, for highly efficient photocatalytic degradation of acetaldehyde at relatively high flow rates. Secondly, the impact of the interaction strength between surface water and the TiO_2 surface on photocatalytic acetaldehyde degradation is studied, providing valuable insights into the role of surface water in the photocatalytic acetaldehyde degradation processes. This is done by preparing a series of anatase TiO_2 with exposed (001) facets but possessing different surface areas and surface properties by applying a solvothermal method. The divergent surface areas and sizes of were achieved by adjusting the solvothermal temperature and solvothermal reaction time. The effect of these synthesis parameters on the structure and physico-chemical properties of TiO_2 was unraveled by different characterization methods such as nitrogen (N_2) sorption, X-ray powder diffraction (XRD), thermogravimetric analyses (TGA) and scanning transmission electron microscopy (STEM), *etc*. Subsequently, these as-prepared titania samples were tested towards photocatalytic degradation of acetaldehyde at relatively high flow rates, *i.e.* 19.25×10^{-3} mL/min (77 ppmv

in a total flow of 250 mL/min) and 16×10^{-3} mL/min (40 ppmv in a total flow of 400 mL/min). The results of photocatalytic acetaldehyde degradation were benchmarked to that of the commercial reference P25 and also compared with results from literature. Additionally, the interaction strength between surface water and the titania surface was studied using diffuse reflectance infrared Fourier transform (DRIFT) measured at different elevated temperatures. The combination of DRIFT, acetaldehyde adsorption, and photocatalytic degradation of acetaldehyde unraveled the impact of the interaction strength between the titania surface and surface water on photocatalytic acetaldehyde degradation. The effect of water was further investigated by varying the humidity during the photocatalytic degradation process. A correlation between the activity of as-prepared TiO_2 samples and their physico-chemical properties was further revealed.

2. Experimental

2.1. Synthesis of TiO_2 catalyst

The mesoporous structures of TiO_2 were obtained using a soft templating method, using F127 as the template in an evaporation-induced self-assembly (EISA) process, resulting in structures with a high surface area [40]. Furthermore, the preferential exposure of (001) facets was targeted by introducing isopropanol and diethylenetriamine to the reaction mixture, which have been shown to selectively coordinate (001) surfaces of anatase, by effectively inhibiting the crystal growth along the [001] direction [41]. In a typical synthesis 1.5 g of F127 (PEO_{106}-PPO_{70}-PEO_{106}, Mw = 12600 g mol^{-1}, Sigma-Aldrich Corp.), 2.29 mL of acetic acid (Sigma-Aldrich Corp.), and 3 mL of concentrated HCl (37%, Sigma-Aldrich Corp.) were mixed, then 30 mL of tetrahydrofuran (THF, Sigma-Aldrich Corp.) were added. After vigorously stirring at 900 rpm for 1 h, 3.58 mL of tetrabutyl titanate (TBOT, Sigma-Aldrich Corp.) was added drop by drop, afterwards 0.2 mL of H_2O was introduced. Then, the obtained transparent light-yellow solution was transferred to a Petri dish and was dried in an oven at 45 °C for 24 h.

Afterwards, 2.5 g of the formed yellow gel was added into 10 mL of anhydrous ethanol (Merck) with stirring at 900 rpm for 1 h to form a homogenous solution. Subsequently, 65 mL of isopropanol (Merck) mixed with 75 μL of diethylenetriamine (99%, Sigma-Aldrich Corp.) were added to the obtained homogenous solution. After complete adding, 15 min of additional stirring was applied to achieve full mixing. The reaction solution was transferred to a 150 mL Teflon-lined stainless-steel autoclave. The reaction temperature was varied from 100 ℃ to 200 ℃ and the reaction time changed between 1 h and 24 h. The autoclave was then taken out from the oven only when the temperature was cooled down to room temperature naturally. Subsequently, the white precipitate was harvested through centrifugation at 4000 rpm for 10 min, followed by five rounds (5 × 30 min) of ethanol washing at the same centrifugation speed to remove organic solvents as much as possible. Afterwards, the precipitate underwent an overnight drying process at 60 ℃. The samples fabricated at different solvothermal temperatures or reaction time were collected together and calcined simultaneously at 550 ℃ in air for 2 h with a ramping rate of 1 ℃/min. Subsequently, these prepared samples were stored in a chamber with desiccant inside to maintain consistent storage conditions. For ease of description, fabricated samples are denoted with their reaction time (at the front) and temperature (at the end). For instance, 100TiO_2-24 indicates that the sample was prepared at 100 ℃ (solvothermal temperature) for 24 h (solvothermal time).

2.2. Preparation of photocatalysts

Before using, soda lime glass slides (2.5 × 1.5 cm^2, VWR) were thoroughly cleaned in a mixture of 70 % sulfuric acid (H_2SO_4, Chem-Lab, 95–97 %) and 30 % hydrogen peroxide (H_2O_2, Chem-Lab) for 30 min. During the preparation, 10 mg of catalyst was dispersed in ethanol (abs. 100 %, Merck), and followed by 30 min of ultrasonication at 30 °C. Afterwards, the well-dispersed solution was casted onto dry glass slides, and then dried in an oven at 80 °C

overnight. In addition, Aeroxide-P25 (Acros Organics) was used as a reference sample without any pretreatment.

2.3. Photocatalytic acetaldehyde activity and acetaldehyde adsorption

The schematic diagram of the entire device for photocatalytic degradation of acetaldehyde is shown in Scheme S1 of the supporting information section. The photocatalytic degradation of acetaldehyde was measured at room temperature in a slit-shaped reactor whose detailed information is available in the earlier work [16,42,43]. Before performing the measurements, the well-dried glass slides coated with catalyst were set in the middle of the reactor. The distance between the surface of catalyst and UVA lamp (Sylvania, 6 W) placed above the reactor was fixed at 4.4 cm, leading to a 1.6 $mW.cm^{-2}$ of light intensity, as measured by an Avantes AvaSpec-3648 spectrometer. For all tests, acetaldehyde was selected as the air pollutant with concentrations set at 77 ppmv and 40 ppmv. During the photocatalytic test, the polluted gas consisted of acetaldehyde (AirLiquide) mixed with dry synthetic air (21% O_2 in N_2, AirLiquide) at a total flow rate of 250 $mL.min^{-1}$ (77 ppmv) or 400 $mL.min^{-1}$ (40 ppmv), respectively. The flow rates of acetaldehyde and air were adjusted by MKS mass flow controllers in the range of 0–200 $mL.min^{-1}$ and 0–2000 $mL.min^{-1}$, respectively. The relative humidity (RH) for the administered gas mixture was 3–5 %, as measured with Sensirion Control Center software. For measurements conducted at a RH of 30 %, another air flow, connected to a mass flow controller within the range of 0–500 $mL.min^{-1}$, was bubbled through a gas wash bottle to adjust the relative humidity levels by controlling the ratio of dry and moist air. Prior to the test, the polluted gas was introduced to the reactor for 40 min to reach the adsorption equilibrium and thus a stable concentration level of acetaldehyde is obtained. Afterwards, the lamp was switched on to illuminate the catalyst for 1 hour to test the samples' reactivity under continuous flow conditions. The variation of concentration of acetaldehyde and CO_2 was monitored in time by FTIR (Thermo Fisher Scientific Nicolet 380 with ZnSe

windows), using the IR bands of acetaldehyde and CO_2 located at 2728 cm^{-1} ($\upsilon_{H-C=O}$ stretching vibration) and 2360 cm^{-1} ($\upsilon_{C=O}$ stretching vibration), respectively. The reason of using these two bands is that they do not interfere with any other species in the FTIR spectrum. Therefore, the changes in concentration could be deduced from the variation of their FTIR band heights using the MacrosBasic software (Thermo Fisher). Finally, the respective concentrations were obtained using pre-established calibration curves. Each acetaldehyde performance test is repeated at least three times to decrease the error of the results.

The stability measurements were performed at 77 ppmv of acetaldehyde at a total flow rate of 250 $mL.min^{-1}$. For the long-time stability measurement, the catalyst was illuminated for 48 h. In an alternative stability experiment, 10 consecutive runs (around 24 h in total) were conducted with light-based regeneration steps in the presence of pure air in-between cycles. The light-based regeneration procedure occurred as follows: After completing one photocatalytic test run, the lamp was turned off while air and acetaldehyde flows remained unchanged. As a result, the acetaldehyde concentration level was restored back to the initial level of around 77 ppmv. Subsequently, the system was purged with air, without acetaldehyde. The lamp was turned on to degrade any remaining pollution from the surface of the samples and within the reactor, under continuous purging with air. This process persisted for 30 min, after which the lamp was again switched off. This concluded the light-based regeneration process. The air flow was redirected to the bypass and mixed with acetaldehyde to again form the polluted test gas, and was reintroduced to the reactor for the photocatalytic measurement. Once the flow of polluted gas stabilized at around 77 ppmv, with a total flow rate of 250 $mL.min^{-1}$ inside the reactor, indicating the adsorption equilibrium was established, the one-hour photocatalytic measurement was initiated. This procedure was repeated during 10 consecutive runs.

The conversion of acetaldehyde is calculated by the Eq. (1),

$$Conversion = [C - C_0]/C_0 \times 100\% \quad (1)$$

The adsorption capacity of acetaldehyde (*i.e.* the amount of acetaldehyde that adsorbs to the surface in dark conditions) is calculated from the concentration time profile during the adsorption equilibrium phase in the dark, prior to the photocatalytic degradation step. The adsorption capacity (A_d) was calculated by the Eq. (2):

$$A_d = C_0 \times \rho_1 \times \rho_2 \times \frac{\left[\int_0^t v\times(1-C/C_0)dt\right]_{catalyst} - \left[\int_0^t v\times(1-C/C_0)dt\right]_{blank}}{m} \quad (2)$$

in which *C* denotes the concentration of acetaldehyde at different time intervals, C_0 represents the initial concentration of acetaldehyde, ρ_1 and ρ_2 refer to the air density and the relative vapor density of acetaldehyde, respectively, *v* represents the acetaldehyde flow rate, and *m* is the weight of the photocatalyst employed in the measurement.

2.4 Characterization

Nitrogen sorption measurements were performed at -196 °C on a Quantachrome Quadrasorb SI automated gas sorption system. Prior to the measurements, a high vacuum degas was carried out on all the samples at 150 °C for 16 h.

Thermal analysis measurements, i.e. thermogravimetric analyses (TGA) and differential thermal analysis (DTG), were performed on a Mettler Toledo TGA-DSC 3+. The parameters used are as follows: a pure oxygen flow of 80 mL/min with a ramping rate of 10 °C /min from 35 °C to 600 °C.

X-ray powder diffraction (XRD) spectra were collected by a D8 advance Eco diffractometer with Cu-Kα radiation (λ= 1.5406 Å) with a scanning range and rate respectively at 10–80 ° 2θ and 0.04 °/4 s.

The diffuse reflectance infrared Fourier transform (DRIFT) measurements were performed using a Nicolet 6700 Fourier Transform IR spectrometer which was equipped with an electromagnetic source in the mid infrared region (4000–400 cm^{-1}) and a DTGS detector. For

the DRIFT measurements from room temperature to 600 °C, a Praying Mantis High Temperature Reaction Chamber (Harrick, USA) was introduced. The specific measurement was done as follows: Prior to measuring the samples, KBr backgrounds were collected at RT after heating at different temperatures for 30 min under a constant Ar flow of 80 mL/min. This cooling-back measurement was to exclude thermal effects on the spectra. After obtaining these backgrounds, a dilution of 2 wt% by KBr was performed on samples. Afterwards, the measurements were carried out at different temperatures, cooling to room temperature to collect spectra (using corresponding background). When collecting a spectrum, the used resolution and accumulation were respectively 4 cm^{-1} and 100.

Scanning Transmission Electron Microscopy (STEM) was performed using High Angle Annular Dark Field (HAADF) detector on the FEI Tecnai Osiris Microscope operating at 200 kV. High resolution HAADF-STEM images were acquired with a probe corrected cubed Thermo Fisher Scientific Titan transmission electron microscope operating at 300 kV with a semi-convergence angle of 21 mrad. The SEM characterization was done with a scanning electron microscope (SEM) equipped with secondary electron and multisegmented backscattered electron detector (SEM, FEI Quanta 250), using an accelerating voltage of 10kV.

3. Results and discussion

3.1 Synthesis and characterization

To obtain TiO_2 with different porous structures and surface areas, the experimental parameters were adjusted, including a variation of the solvothermal temperature from 100 ℃ to 200 ℃ at a constant reaction time of 24 h and a change in reaction time from 1 h to 24 h at a constant solvothermal temperature of 180 ℃. Nitrogen adsorption-desorption isotherms were collected to evaluate the changes in pore structure, pore size distribution, and surface area, as displayed in Fig. 1. The crystal phase of samples was determined using XRD, as illustrated in

277 Fig. 2. The data obtained from nitrogen sorption and XRD are summarized in Table 1.
278 Additionally, Table 1 also includes the specific information about the synthesis.

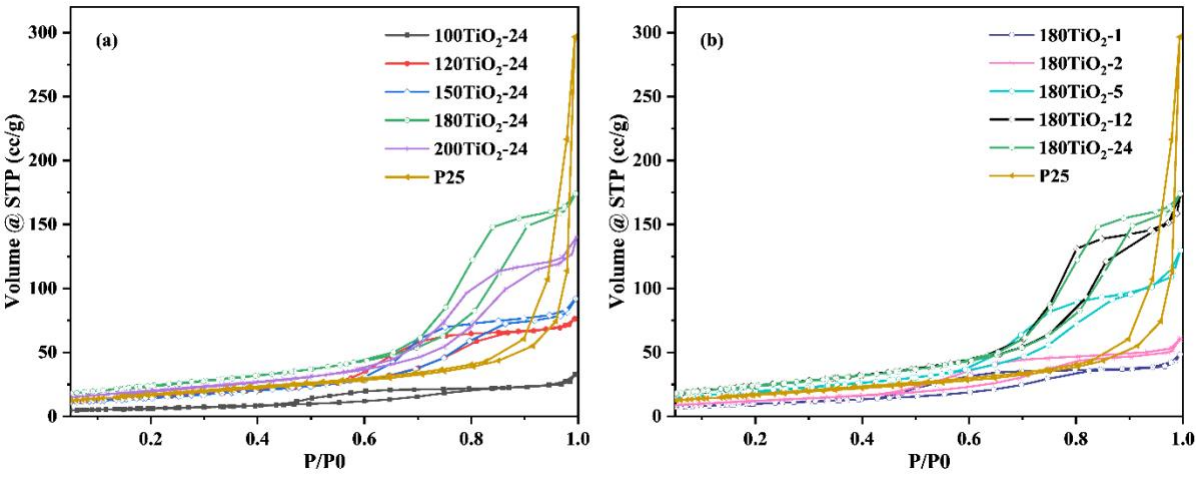

279

280 Fig. 1. Nitrogen adsorption-desorption isotherms of P25 and prepared TiO_2 samples. (a) TiO_2 prepared
281 at 100–200 °C for 24 h; (b) Samples fabricated at 180 °C for 1–24 h.

282 Fig. 1a-b shows the nitrogen adsorption-desorption isotherms for as-prepared samples and
283 P25. All provided nitrogen isotherms of prepared samples are classified to IUPAC IV(a) and
284 show H1 hysteresis loops [44], indicating a mesoporous structure. A type H3 hysteresis was
285 observed in P25, moreover, the position of the hysteresis is close to $P/P_0 = 1$, indicating the
286 presence of macropores. However, P25 is nonporous, synthesized by hydrolysis of $TiCl_4$ in a
287 hydrogen flame [45]. Therefore, the macropores are ascribed to the inter-particle porosity.
288 Based on nitrogen adsorption-desorption isotherms, the BET-SSA (specific surface area) of
289 P25 and prepared TiO_2 samples was calculated and summarized in Table 1. Except $100TiO_2$-
290 24, $180TiO_2$-1, and $180TiO_2$-2, the remaining as-prepared TiO_2 samples exhibited similar or
291 higher specific surface areas than commercial P25. When the solvothermal reaction time was
292 kept constant at 24 h, no evident trend was observed between the BET-SSA of as-fabricated
293 TiO_2 and solvothermal temperature. At a solvothermal temperature of 180 °C, the BET-SSA
294 of as-prepared TiO_2 samples increased as the solvothermal time increased. Moreover, samples
295 $180TiO_2$-12 and $180TiO_2$-24 exhibited nearly identical BET-SSA values, within the
296 experimental error. Additionally, the pore volumes of as-prepared samples are listed in Table

1. The changes in pore volume of prepared TiO_2 samples corresponded directly to the variations in BET-SSA. This is intuitively represented in Fig. S1, which illustrates the specific correlation between the pore volume and BET-SSA. The role of the solvothermal reaction time and temperature in surface areas or pore volumes will be discussed later.

In addition, the variations in pore size distribution (PSD, determined using the Barrett-Joyner-Halenda method), obtained based on the desorption branch of as-fabricated samples are displayed in Fig. S2. The pore size distribution of all the as-prepared TiO_2 samples falls within the range of mesopores (2–50 nm), confirming the presence of mesoporous structures. At a solvothermal time of 24 h, the TiO_2 samples showed a broader PSD and larger finest pore size as the solvothermal temperature increased. Moreover, the finest pore size was smaller for $200TiO_2$-24 compared to $180TiO_2$-24, while their PSDs were similar. Similarly, at a constant solvothermal temperature of 180 ℃, increasing the solvothermal reaction time resulted in a broader PSD and larger finest pore sizes. Furthermore, sample $180TiO_2$-24 exhibited a similar finest pore size and a broader PSD compared to sample $180TiO_2$-12.

The presence of a mesoporous structure and a large surface area are dominant driving forces for photocatalytic acetaldehyde degradation. These factors can enhance the mass transfer during acetaldehyde degradation and more active sites can be exposed over the surface, resulting in improved acetaldehyde removal efficiency [22,27,28].

Table 1. Physico-chemical characteristics of P25 and as-prepared TiO_2.

Sample name	Temp. of solvothermal (°C)	Period of solvothermal (h)	BET surface area (m^2/g)	Crystallite size (nm)	Pore volume (cc/g)	Crystal phase
100TiO₂-24	100	24	23	21.2	0.04	Anatase
120TiO₂-24	120	24	55	18.1	0.11	Anatase
150TiO₂-24	150	24	54	18.3	0.12	Anatase
180TiO₂-24	180	24	88	14.5	0.25	Anatase
200TiO₂-24	200	24	75	15.9	0.19	Anatase
180TiO₂-12	180	12	89	14.6	0.23	Anatase
180TiO₂-5	180	5	72	16.6	0.18	Anatase
180TiO₂-2	180	2	45	19.3	0.08	Anatase
180TiO₂-1	180	1	36	20.4	0.06	Anatase
P25	-	-	55	20.2	-	Anatase (80%) and rutile (20%)

321 The experimental errors for surface area and crystallite size are respectively 10 % and ± 0.2 nm.

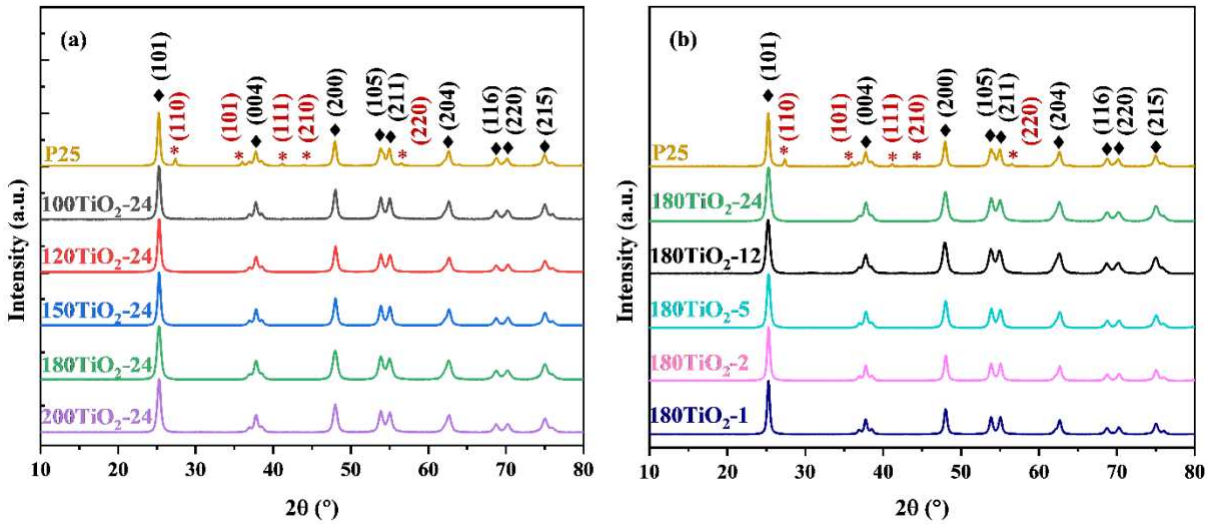

322

323 Fig. 2. XRD patterns of P25 and TiO_2 samples prepared at 100–200 °C for 24 h are in (a), of P25 and

324 those fabricated at 180 °C for 1–24 h are in (b). ♦ is for anatase, * is for rutile.

Fig. 2 displays the XRD patterns of commercial P25 and fabricated samples. The commercial P25 shows the mixed phases of anatase and rutile and its pattern corresponds to the patterns in JCPDS No. 21-1272 (anatase) and No. 21-1276 (rutile) [46,47] (Fig. 2). The peaks of anatase at 25.2°, 37.6°, 48.0°, 53.7°, 55.0°, 62.6°, 68.5°, 70.2° and 74.9° correspond to the planes of (101), (004), (200), (105), (211), (204), (116), (220), and (215). The pattern of rutile phase exhibits peaks at 27.4°, 36.0°, 41.0°,44.0°, and 56.6°, which are respectively attributed to the reflection planes of (110), (101), (111), (210) and (220). Irrespective of the solvothermal temperature and time, all the prepared TiO_2 samples showed well-defined crystallization of only anatase phase. The average crystallite size of all TiO_2 samples in Table 1 was estimated based on the most pronounced diffraction peak of the (101) plane, using the Scherrer equation [48]. Most of the as-prepared titania exhibited a smaller crystallite size than P25, except $100TiO_2$-24 and $180TiO_2$-1. Moreover, the changes in crystallite size observed in the as-prepared TiO_2 samples are related to the variations in surface area, as also reported in literature [49–51]. This is intuitively represented in Fig. S1, which illustrates the correlation between the crystallite size and BET-SSA.

At a solvothermal temperature of 180 °C, the solvothermal reaction time is related to the ultimate crystallite size, surface area, and pore volume of the titania samples. It can be expected that with increasing solvothermal time, more nucleation events are allowed to occur, resulting in smaller crystallite sizes and consequently larger surface areas and pore volumes. When the solvothermal time was kept constant (24 h), the solvothermal temperature could also affect the resulting crystallite size, surface area, and pore volume of the samples. A higher temperature appears to lead to titania species with a smaller crystallite size, higher surface area and pore volume, although no evident correlation was found. A higher solvothermal temperature could promote nucleation, and formed particles could also re-dissolve under these conditions, leading

to a smaller crystallite size and, consequently, a higher surface area and pore volume. However, more specific underlying reasons for this remain unclear with the information at hand.

A small crystallite size is widely accepted as an important factor that promotes photocatalytic acetaldehyde degradation. The combination of a mesoporous structure, a relatively large surface area, and small crystallite size, which is present in some as-prepared TiO_2 samples, provides significant advantages for enhancing the photocatalytic efficiency of acetaldehyde degradation. Consequently, these TiO_2 samples are expected to exhibit highly efficient photocatalytic acetaldehyde degradation.

3.2 Hydroxyl groups and surface water

It is well known that the hydroxyl groups and surface-bound water on TiO_2 play a significant role in the degradation of contaminants [27,52,53]. This is because OH groups provide the reactive sites for acetaldehyde (and intermediate) adsorption. On the other hand, acetaldehyde adsorption competes with water sorption at these sites. An appropriate content of surface water is beneficial for the photocatalytic degradation of acetaldehyde by acting as a source of ·OH radicals upon illumination. When there is excessive surface water, however, the activity of TiO_2 can be potentially suppressed. This study will further investigate the effect of variations in the surface water-TiO_2 surface interaction strength on the resulting photocatalytic acetaldehyde degradation. Here, the OH groups and surface water on P25 and as-prepared samples were characterized by DRIFT, identifying the presence of hydroxyl groups and surface-bound water and determining the interaction strength between surface water and the TiO_2 surface. The TG/DTG technique was applied to estimate the amount of surface water and OH groups on the TiO_2 surfaces.

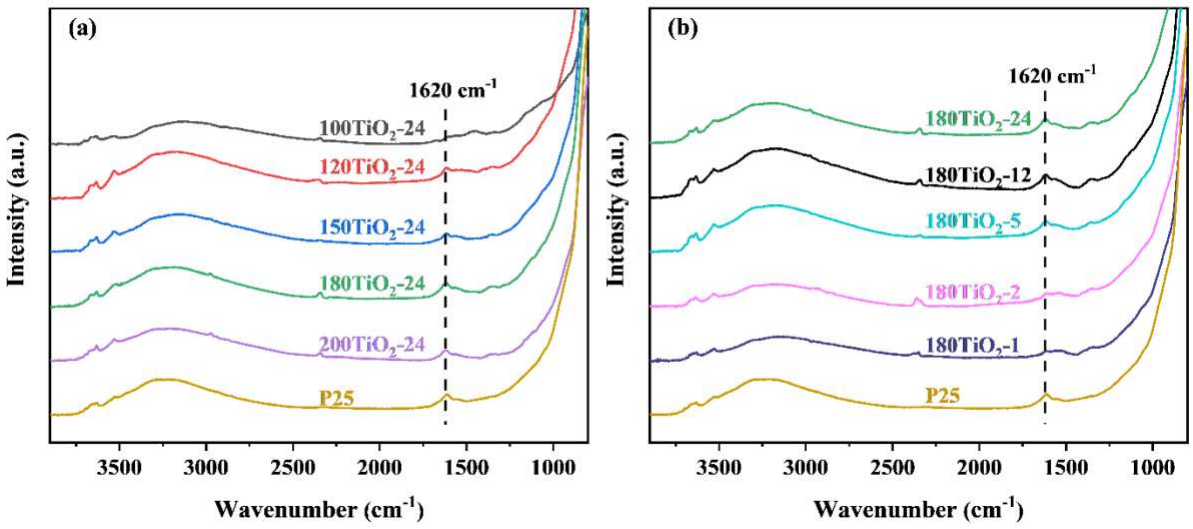

371

372 Fig. 3. DRIFT spectra of as-prepared TiO_2 and commercial P25, as measured under an argon flow of
373 80 mL/min at room temperature. (a) P25 and TiO_2 samples prepared at 100–200 °C for 24 h; (b) P25
374 and TiO_2 samples fabricated at 180 °C for 1–24 h.

375 To identify the hydroxyl groups and surface water on TiO_2 samples, DRIFT spectra were
376 collected at room temperature, as seen in Fig. 3. The existence of surface hydroxyl groups
377 (3700–2500 cm^{-1}) and surface water (1620 cm^{-1}) were observed on as-prepared titania samples
378 and commercial P25 [27]. Among these OH groups, the bands at 3700–3600 cm^{-1} are assigned
379 to the hydroxyl groups on the titania surface, while the broad band at 3600–3000 cm^{-1} is
380 ascribed to the overlapping signals of adsorbed water and the stretching of OH groups [54].
381 Although these titania samples exhibit similar signals of hydroxyl groups, the different
382 intensity ratios on these samples might suggest different distributions or number of OH groups,
383 which could represent different surface properties and thus play different roles in the
384 degradation of acetaldehyde. Furthermore, almost no obvious bands which are related to
385 organic compounds were observed on as-prepared titania samples, indicating that the F127
386 template was fully removed during the calcination process.

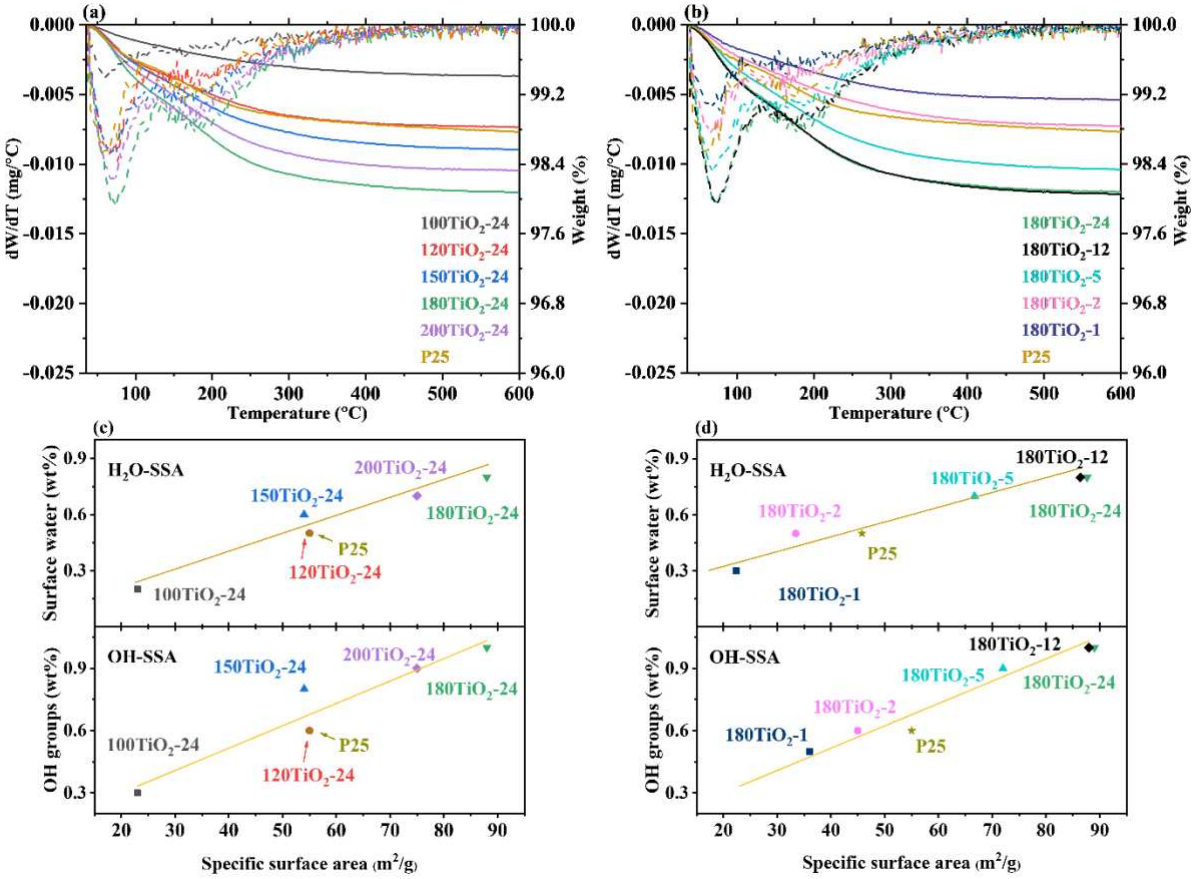

Fig. 4 TG/DTG results for (a) P25 and TiO_2 samples prepared at different solvothermal temperatures (100 – 200 °C) for 24 h and (b) P25 and TiO_2 samples synthesized at 180°C for different solvothermal reaction times (1 – 24 h). Panels (c) and (d) display the correlations between the amount of surface water, hydroxyl groups, and specific surface area (SSA) of these sample sets, respectively. The dashed and full lines are for DTG and TG curves, respectively.

To estimate the content of hydroxyl groups and surface water on the TiO_2 samples, TGA measurements were performed from 35 °C to 600 °C under a pure oxygen flow of 80 mL/min, as shown in Fig. 4a-b. The results show two noticeable weight losses and corresponding DTG maxima for all samples: one from room temperature to 130 °C and another one from 130 °C to 400 °C. The weight loss at RT to 130 °C can be attributed to surface water desorption, while the majority of weight loss from 130 °C to 400 °C is due to the condensation between OH groups (possibly including desorption of some strongly adsorbed surface water) [27,55,56]. Therefore, the content of surface water and hydroxyl groups in these TiO_2 samples could be estimated based on the weight losses observed within these two temperature ranges. More

detailed data can be found in Table S1. Fig. 4c-d depict the correlations between the hydroxyl group content and surface area, as well as the surface water content and surface area. OH groups, as one of the active sites for acetaldehyde adsorption, show an increasing content with increasing surface area. That is, higher surface areas provide more active sites for acetaldehyde adsorption, potentially leading to better acetaldehyde degradation efficiency. Similarly, the increased content of surface water with the increase in surface area could lead to a higher rate of OH radical formation during illumination, thereby promoting the degradation process. Moreover, Fig. 4a-b shows that all as-prepared samples exhibit almost no weight loss above 400 °C, and their total weight loss between RT–600 °C was the sum of the lost surface water and hydroxyl groups (see Table S1). This again confirms that the template was successfully removed during the calcination, which is consistent with the DRIFT results above.

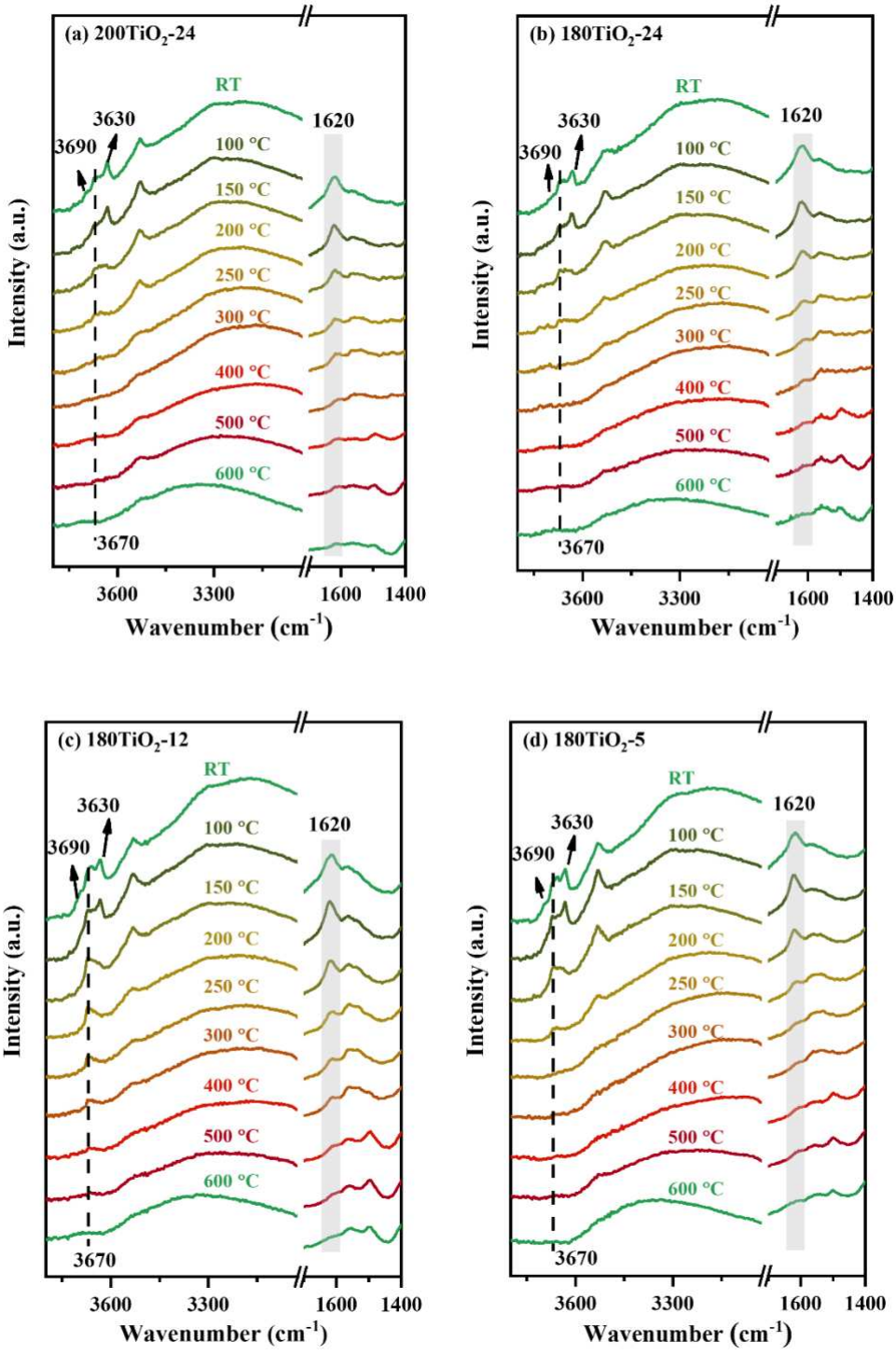

Fig. 5. DIRFT spectra of as-prepared TiO_2, as measured under an argon flow of 80 mL/min from room temperature to 600 °C. (a) 200TiO_2-24, (b) 180TiO_2-24, (c) 180TiO_2-12, (d) 180TiO_2-5.

In order to clarify the differences in the interaction strength between surface water and TiO_2 surface, the DRIFT spectra were collected from 30 °C to 600 °C under an Ar flow. Samples 180TiO_2-24, 200TiO_2-24, 180TiO_2-12 and 180TiO_2-5 were selected as they display similar and higher surface area than other samples, as seen in Fig. 5. The DRIFT spectra of other samples

420 can be found in Fig. S3. With increasing temperature, all samples display a decreasing intensity
421 for hydroxyl groups (3670 cm^{-1} and 3600–3000 cm^{-1}) and surface-bound water (1620 cm^{-1}),
422 indicating the condensation of OH groups and the desorption of surface-bound water. Other
423 bands at 3630 cm^{-1} and 3690 cm^{-1}, which are assigned to OH hydrogen-bonded to surface water
424 and the stretching mode of water with dangling H, respectively, also became small with the
425 desorption of surface water [27,54]. Furthermore, titania samples in Fig. 5 all displayed
426 different surface water desorption temperatures, suggesting different interaction strengths
427 between surface water and the titania surface. This probably leads to different degrees of
428 competitive adsorption between surface water and acetaldehyde onto the titania surface. The
429 spectra of 200TiO_2-24 (Fig. 5a) show that the signal of surface water at 1620 cm^{-1} becomes
430 almost unresolved at 300 °C and its intensity does not decrease anymore with further increase
431 in temperature. Therefore, the complete desorption of adsorbed surface water was at 300 °C
432 for 200TiO_2-24. Similarly, the desorption temperatures of surface-bound water on 180TiO_2-24,
433 180TiO_2-12 and 180TiO_2-5 were at 400 °C (Fig. 5b), 400 °C (Fig. 5c), and 250 °C (Fig. 5d),
434 respectively. A lower desorption temperature of surface-bound water indicates a weaker
435 interaction strength between surface water and the TiO_2 surface, which probably results in a
436 weaker competitive interaction between surface water and acetaldehyde for adsorption on
437 titania. Therefore, the varying interaction strengths between surface water and the TiO_2 surface
438 in different samples might indicate that the affinity between the TiO_2 surface and acetaldehyde
439 could vary from sample to sample, resulting in divergent acetaldehyde adsorption capacities.
440 Consequently, the 180TiO_2-5 surface exhibits the weakest interaction strength with adsorbed
441 surface water among those samples, letting us assume that acetaldehyde might adsorb more
442 easily to its surface, thereby improving the acetaldehyde adsorption capacity and potentially
443 enhancing the photocatalytic acetaldehyde degradation efficiency.

Additionally, Table S1 summarizes the desorption temperature of surface-bound water over different TiO_2 samples. No clear correlation was found between the desorption temperature of surface-bound water and solvothermal temperature or solvothermal reaction time.

3.3 Morphology

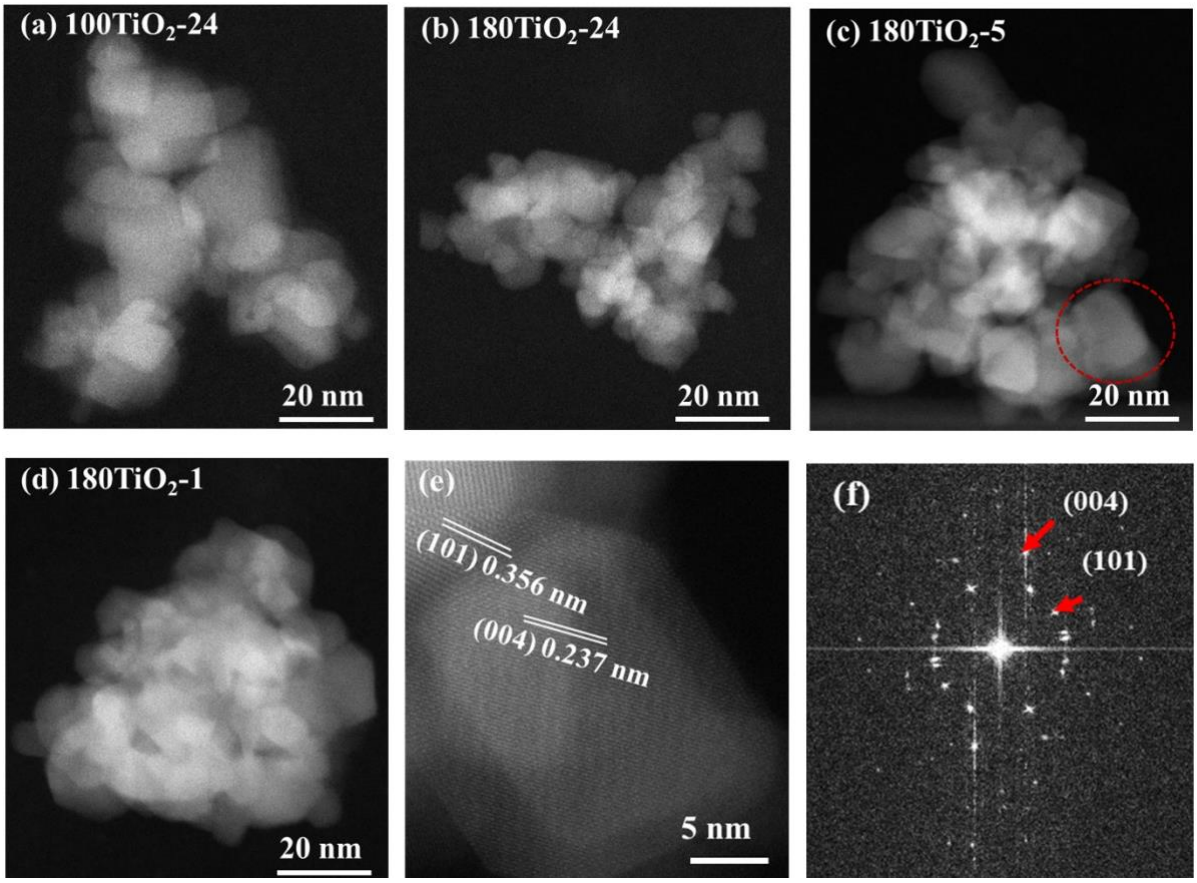

Fig. 6. HAADF-STEM (a-d) and high resolution HAADF-STEM (e) images of as-prepared TiO_2. (e) Enlarged from the dotted red-circle area in (c), (f) is its corresponding FFT pattern.

HAADF-STEM was applied to characterize the facets of as-prepared TiO_2. Samples $100TiO_2$-24, $180TiO_2$-24, $180TiO_2$-5, and $180TiO_2$-1 were selected, as shown in Fig. 6a-d, respectively. Sample $180TiO_2$-5 was selected to be further analyzed by high resolution HAADF-STEM image (Fig. 6e) and fast Fourier transform (FFT) patterning (Fig. 6f). The results display top facet planes with a lattice spacing of 0.237 nm, and an interplanar spacing of 0.356 nm was paralleled to the side facets, corresponding to the (004) and (101) planes of anatase with exposed (001) facets [57,58]. Therefore, it could be deduced that predominantly

458 (001) facets were exposed on all these presented samples, irrespective of the reaction time and
459 temperature. The emerging (001) facets could be due to the stabilization effect by
460 diethylenetriamine and isopropanol in the solvothermal process, as they prevent crystal growth
461 along the [001] direction, which has been reported in literature [59,60]. In principle there could
462 be a correlation between the percentage of exposed (001) facets and reaction time or
463 temperature. However, we have not attempted to estimate this since the particle size among as-
464 prepared TiO_2 samples is not sufficiently uniform (see Fig. S4, 100TiO_2-24 even did not show
465 spherical nanoparticles). This could be induced by the polar solvent, the mixture of isopropanol
466 and ethanol. The Ostwald ripening or sequential nucleation tends to take place in polar solvents,
467 resulting in a broader distribution of particle size [61]. Even though most prepared samples
468 consist in fact of spherical shaped nanoparticles (except for 100TiO_2-24), their particle size
469 does not show a clear correlation with solvothermal time or temperature. The nanocrystal size
470 of these as-prepared TiO_2 samples ranged from 5–15 nm, which is relatively small compared
471 to values reported in the literature [62–65]. This small size is beneficial for enhancing the
472 reactivity of (001) facets. It is known that (001) facets on anatase are more reactive than the
473 thermodynamically stable (101) facets, and can thus boost the degradation efficiency of VOCs
474 [38,39]. Therefore, it is expected that the as-prepared TiO_2 samples will show further improved
475 acetaldehyde degradation performance due to the combination of preferential exposure of (001)
476 facets and small size of nanocrystals.

477 **3.4 Photocatalytic activity**

478 The photodegradation, conducted without samples inside the reactor, and photocatalytic
479 degradation of acetaldehyde using different TiO_2 samples, were run at an inlet concentration
480 of *ca*. 77 ppmv of acetaldehyde in air at a total flow rate of 250 mL/min. Fig. 7a represents a
481 blanc control experiment, in which bare glass slides were placed inside the reactor without
482 TiO_2. The concentration of acetaldehyde briefly dropped after introducing the gas flow to the

reactor due to air displacement. When the light was switched on, the concentration of acetaldehyde remained constant, suggesting no acetaldehyde degradation. Therefore, UV light alone is insufficient for acetaldehyde degradation.

Fig. 7b shows the results of photocatalytic degradation of acetaldehyde over TiO_2 samples fabricated with the same reaction time (24 h) but at different solvothermal temperatures (100–200 °C) and P25. When the lamp was switched on to illuminate the catalyst, the concentration of acetaldehyde is first observed to slightly increase, and then rapidly decreases until leveled off. Fig. 7b shows that except for sample $100TiO_2$-24, other TiO_2 samples display better acetaldehyde degradation performance than P25, with $180TiO_2$-24 showing the best performance. Three samples ($120TiO_2$-24, $150TiO_2$-24 and $200TiO_2$-24) present a similar degradation efficiency, which was lower than $180TiO_2$-24 and higher than P25. The superior performance of these samples compared to P25 derive their effect from a combination of positive factors, such as a more porous structure, smaller crystallite size and/or higher BET-SSA as well as more surface hydroxyl groups. The crystallite size, surface area and hydroxyl group content reached the lowest and highest values, respectively, for the sample prepared at 180 °C, which is therefore expected to yield the best acetaldehyde degradation performance [66,67]. Moreover, the presence of (001) facets on as-prepared samples could also contribute to the improvement of photocatalytic acetaldehyde degradation.

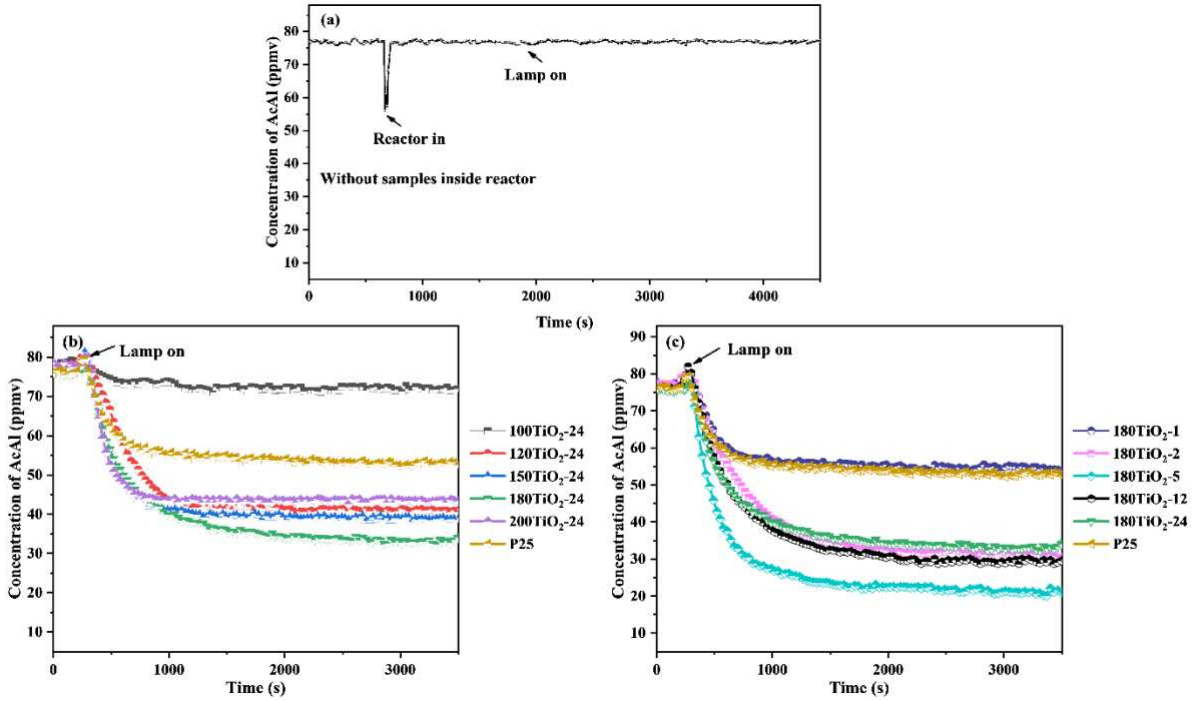

Fig. 7. Photodegradation of acetaldehyde without titania inside the reactor (a), and photocatalytic degradation of acetaldehyde (AcAl) over different samples (b-c). All the measurements were performed under UV light illumination, at an around 77 ppmv of acetaldehyde in dry air (RH = 3–5 %) at a total flow rate of 250 mL/min. (b) P25 and TiO_2 samples prepared at 100–200 °C for 24 h; (c) P25 and TiO_2 samples fabricated at 180 °C for 1–24 h.

Fig. 7c plots the results of photocatalytic degradation of acetaldehyde over samples prepared at the same temperature (180 °C) but with different reaction time (1–24h) and P25. 180TiO_2-5 degraded acetaldehyde better than TiO_2 prepared during other periods (1 h, 2 h, 12 h and 24 h), showing a conversion of around 74 %. Although 180TiO_2-5 showed that the positive impact factors, e.g. pore volume, surface area and the content of hydroxyl groups, almost reached the highest values, it additionally displayed a larger crystallite size than other samples, which is again assumed to be disadvantageous. Therefore, the positive impact factors apparently outweigh the effect of crystallite size in this case. Its lower desorption temperature of surface water, designating a weaker interaction between surface water and the titania surface, indicates that the competitive interaction between the adsorbed surface water and acetaldehyde towards the titania surface might also be weaker. Therefore, acetaldehyde might adsorb onto 180TiO_2-5 more easily, which could induce a higher acetaldehyde degradation efficiency. Moreover, the

519 photocatalytic degradation efficiency of acetaldehyde does not show a clear trend for the
520 remaining as-prepared TiO_2 samples. Therefore, no further in-depth analysis is provided.
521 However, it can still be anticipated that the aforementioned influencing factors collectively
522 impact their photocatalytic acetaldehyde efficiency.

523 Photocatalytic acetaldehyde degradation on TiO_2 involves various possible reaction
524 pathways. It is widely accepted that the process begins with the adsorption of acetaldehyde
525 onto the TiO_2 surface, followed by degradation facilitated by photogenerated hydroxyl radicals
526 (from H_2O) and superoxide radicals (from O_2) [36]. Our earlier work explored the
527 photocatalytic degradation pathway of acetaldehyde on TiO_2 using *operando* FTIR
528 spectroscopy [8]. Consistent with literature [36], the adsorption process involves both aldol
529 condensation and a minor oxidation, resulting in the formation of 3-hydroxybutanal and
530 crotonaldehyde, as well as acetate. The adsorption on anatase predominantly involves the aldol
531 condensation, resulting in the formation of crotonaldehyde. With the illumination of UV light,
532 crotonaldehyde is converted to intermediates acetic acid and formic acid, eventually producing
533 CO_2 and H_2O, or is directly mineralized to CO_2. The pathway of acetaldehyde decomposition
534 on anatase was found to be more efficient in generating CO_2 compared to that on rutile [22,36].
535 The full reaction pathway of acetaldehyde to CO_2 and all possible intermediates, is given in the
536 study of Hauchecorne et al. [8].

537 To evaluate the selectivity of acetaldehyde degradation in this study, Fig. 8 presents the
538 concentrations of converted acetaldehyde and generated CO_2 over as-prepared TiO_2 samples
539 and P25 during the photocatalytic process. It is evident that the concentration of generated CO_2
540 is approximately two times that of converted acetaldehyde for all the samples, suggesting that
541 the photocatalytic acetaldehyde mineralization process is quite selective. In addition, Fig. S5
542 illustrates the real-time detection of acetaldehyde, generated CO_2 and H_2O under steady state
543 conditions during the photocatalytic process. In the FTIR spectra, all the as-prepared TiO_2

samples and P25 exhibit that there is nothing else in the gas phase spectrum other than unconverted acetaldehyde, and CO_2 and H_2O as mineralization products. If any other organic by-products such as acetic acid would be formed, their contribution is expected to be insignificant and below the detection limit. This further confirms that CO_2 and H_2O are the main ultimate products in the photocatalytic degradation of acetaldehyde, and the selectivity of acetaldehyde is nearly 100 % for all TiO_2 samples. The selectivity in this study is similar with findings from literature [27–29,68].

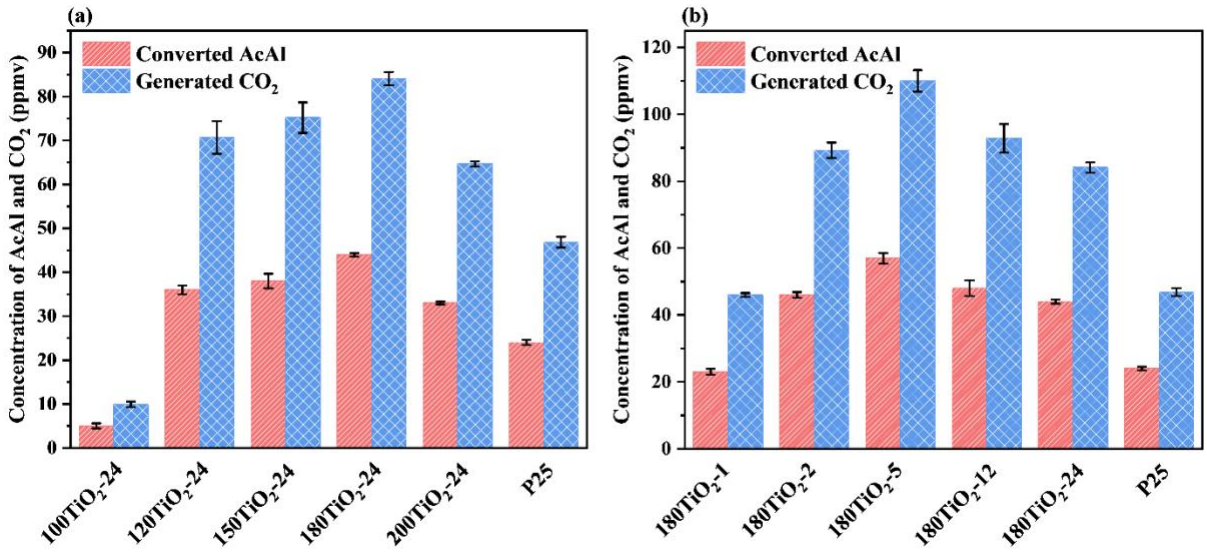

Fig. 8. Concentrations of converted acetaldehyde (AcAl) and generated CO_2 over different samples during the photocatalytic degradation of acetaldehyde, measured at 77 ppmv of acetaldehyde in dry air (RH = 3–5 %) at a total flow rate of 250 mL/min. (a) P25 and TiO_2 samples prepared at 100–200 °C for 24 h, (b) P25 and TiO_2 samples fabricated at 180 °C for 1–24 h. The error bars were obtained from standard errors based on three repeated measurements.

The acetaldehyde adsorption capacity on P25 and as-prepared TiO_2 samples was calculated as the amount of acetaldehyde taken up by the sample when introducing the polluted gas stream to the reactor in dark conditions, resulting in a decrease of the outlet concentration due to adsorption, until the outlet concentration returns to the bypass reference level indicating that the adsorption-desorption equilibrium has been reached. Based on the changes in acetaldehyde adsorption capacity, a correlation between this and the AcAl conversion efficiency was found,

564 as shown by the blue icons in Fig. 9a-b. It is evident that samples with high acetaldehyde
565 adsorption capacities correspond to high acetaldehyde conversions. The acetaldehyde
566 adsorption capacity is largely determined by the number of active sites. A large surface area,
567 which can expose more active sites, thus logically results in a higher acetaldehyde adsorption
568 capacity [22,27]. Among the photocatalytic degradation of acetaldehyde tests, the best-
569 performing sample, 180TiO_2-5, exhibits the highest acetaldehyde capacity although not having
570 the largest specific surface area. This indicates that 180TiO_2-5 has stronger surface affinity for
571 acetaldehyde. This finding provides evidence for the conclusion obtained from the DRIFT
572 experiment in Fig. 5, where 180TiO_2-5 showed the weakest competitive interaction between
573 surface water and acetaldehyde for adsorption, compared to other good-performing samples
574 (180TiO_2-12, 180TiO_2-24, 200TiO_2-24). Therefore, the weak interaction strength between the
575 titania surface and surface water reduces the competitive adsorption of acetaldehyde and water
576 onto titania, thereby promoting the acetaldehyde adsorption, and ultimately improving the
577 acetaldehyde degradation. Likewise, this finding is also applicable to comparisons among other
578 samples, such as 180TiO_2-2, 120TiO_2-24, 150TiO_2-24, and P25. Apart from that, the specific
579 surface area of the samples relates to the acetaldehyde conversion as well, as indicated by the
580 black icons in Fig. 9a-b. High surface area samples can be expected to exhibit a high
581 acetaldehyde conversion, although not in an absolute manner. The correlation between the
582 surface area and acetaldehyde conversion is also consistent with literature [22,27].

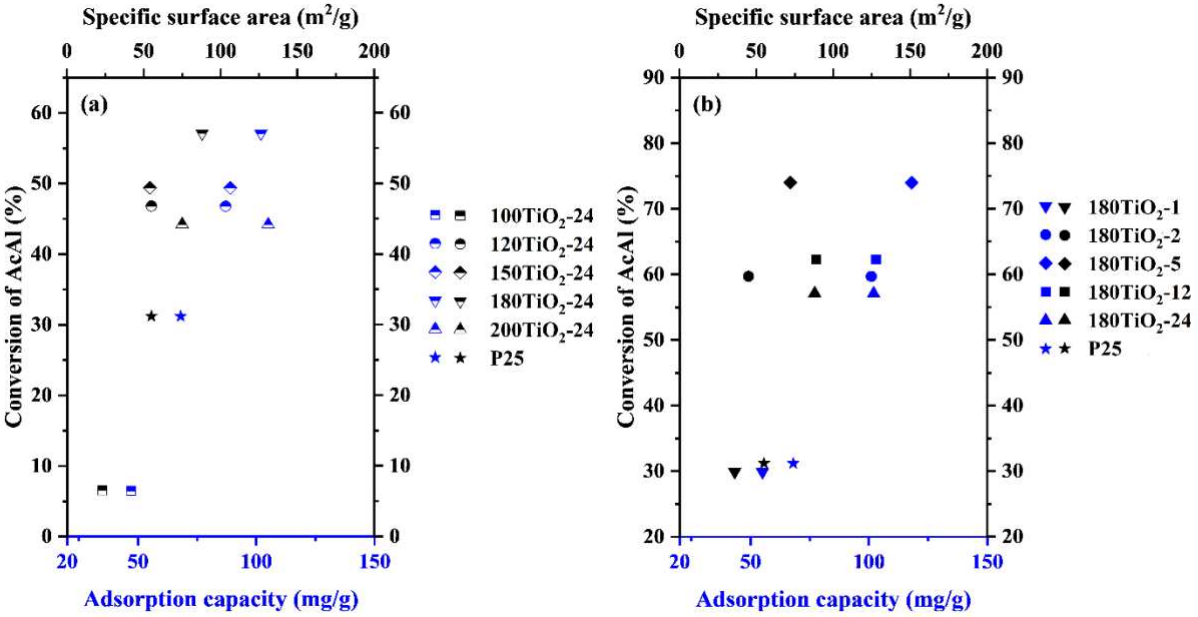

Fig. 9. Correlation of acetaldehyde (AcAl) conversion with specific surface area and acetaldehyde adsorption capacity. (a) P25 and TiO_2 samples prepared at 100–200 °C for 24 h; (b) P25 and TiO_2 samples fabricated at 180 °C for 1–24 h.

Table 2 lists the photocatalytic performance of acetaldehyde degradation of TiO_2 samples reported in literature, including the results of this study. These measurements were conducted under UV at room temperature, utilizing different measurement parameters such as sample weight, flow rate of acetaldehyde, lamp intensity, *etc*. As the acetaldehyde conversion is influenced by both the inlet concentration (ppmv) and the total flow rate (mL/min), we decided to calculate and report the acetaldehyde flow rate to compare the photocatalytic performance of samples in different studies. High sample weights, low acetaldehyde flow rates, and high lamp intensities typically promote the photocatalytic degradation efficiency. Table 2 demonstrates that the best-performing sample synthesized in this study ($180TiO_2$-5) exhibits the highest acetaldehyde degradation efficiency compared to the samples reported in literature. It achieves a conversion of 100 % at an acetaldehyde flow rate of 16×10^{-3} mL/min and 74 % at a flow rate of 19.25×10^{-3} mL/min, *i.e.* the highest conversion of acetaldehyde even at higher flow rates. Moreover, this sample was measured under even more challenging conditions, *i.e.* a smaller amount of photocatalyst (4–20% of the sample amount used in the literature, if

602 reported) and a lower lamp intensity (3–8 % of intensity used in other studies, if reported). The
603 excellent performance of the as-prepared titania underscores its significant potential in the
604 photocatalytic degradation of acetaldehyde.

605 Table 2. A comparison of photocatalytic acetaldehyde (AcAl) degradation performance of TiO_2 in
606 literature and this study (180TiO_2-5), measured under UV light at ambient temperature (25–30 °C) using
607 different measurement parameters (e.g., sample mass, flow rate of acetaldehyde, lamp intensity, *etc*.).

Reference	Sample weight (mg)	Flow rate of AcAl (1×10^{-3} mL/min)	Lamp intensity (mW/cm^2)	Conversion of AcAl (%)
TiO_2 (Fig. 7c, this work)	10	19.25	1.6	74 ± 1
TiO_2 (Fig. S6, This work)	10	16	1.6	100
TiO_2 [69]	100	0.5	51.2	99.2
TiO_2 [29]	50	4	50	92
TiO_2 [70]	110	6	u.n	35
TiO_2 [71]	u.n	1	20	55
TiO_2 [72]	u.n	5	u.n	100
TiO_2 [3]	250	12.06	u.n	100

608

609 Additionally, the stability of the prepared TiO_2 sample was confirmed by running ten
610 consecutive photocatalytic tests (around 24 h in total) as well as one long-time (48 h)
611 measurement on the best performing sample (180TiO_2-5), as seen in Fig. 10a-b. Fig. 10a shows
612 the results of ten consecutive runs, with “lamp on” and “lamp off” periods displayed by the
613 light blue and dark blue lines, respectively. Within one run of the measurement in Fig. 10a,
614 when the lamp was turned on, the concentration of acetaldehyde rapidly decreased until
615 levelled off (light blue line); when the lamp was turned off, the acetaldehyde concentration

quickly rose again until it reached the initial concentration (dark blue line). The acetaldehyde degradation efficiency remained almost the same after ten runs. Fig. 10b presents one long-term stability test. The results indicate that the sample maintains a very constant activity towards acetaldehyde degradation over a 48-hour time span. Both experiments thus confirm the superior stability of the highly performant 180TiO_2-5 sample.

There always was a light-based regeneration step with pure air in-between cycles in the consecutive tests. Such a step is depicted in Fig. 10c. After completing one photocatalytic test run, the lamp was turned off while air and acetaldehyde flows remained unchanged. As a result, the acetaldehyde concentration level was restored back to the initial level of around 77 ppmv. Subsequently, the system was purged with air, without acetaldehyde. The lamp was turned on to degrade any remaining pollution from the surface of the samples and within the reactor, under continuous purging with air. This process persisted for 30 min, after which the lamp was again switched off. This concluded the light-based regeneration process. The air flow was redirected to the bypass and mixed with acetaldehyde to again form the polluted test gas, and was reintroduced to the reactor for the photocatalytic measurement. The processes of light-based regeneration, gas mixing in bypass, and the reintroduction of the polluted gas to the reactor were not shown in Fig.10a.

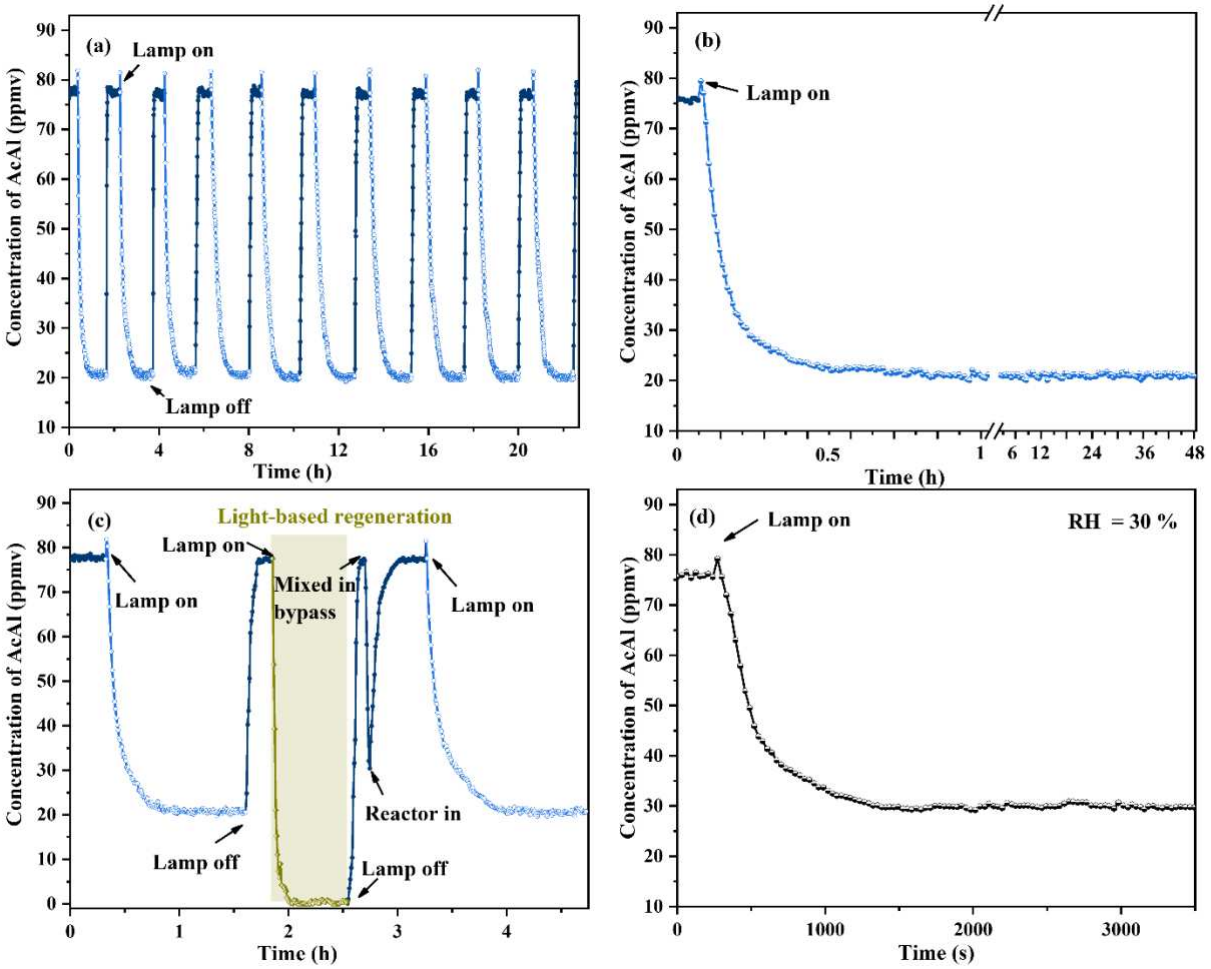

Fig. 10. Photocatalytic degradation of acetaldehyde (AcAl) over 180TiO_2-5, measured by (a) running ten consecutive tests and (b) one 48-hour long-term test at ~77 ppmv of acetaldehyde in dry air (RH = 3–5 %) at a total flow rate of 250 mL/min. (c) Two consecutive tests as shown in (a), demonstrating the processes of light-based regeneration, gas mixing, and the reintroduction of polluted gas. The dark blue lines represent AcAl concentrations before and after the photocatalytic degradation, the light blues lines are for the changes in AcAl concentration during the photocatalytic process, the dark yellow lines represent the light-based regeneration process. (d) A measurement conducted at a relative humidity of 30 % at the same concentration of acetaldehyde and total flow rate.

The relative humidity level of indoor air is recommended to be between 30–50 % by the EPA (Environmental Protection Agency). To confirm the feasibility of employing the as-prepared TiO_2 sample in a realistic humid environment, measurements were also performed at a RH of 30 %, as shown in Fig. 10d. At an acetaldehyde concentration of 77 ppmv and a total flow rate of 250 mL/min, the conversion of acetaldehyde decreased from approximately 74 % (for dry air, RH of 3–5 %, Fig. 10a-b) to 61 % under the RH of 30 %. Hence, 82 % of the activity is

retained at a higher humidity level. On the one hand, the decrease in the conversion of acetaldehyde demonstrates the inhibiting effect of excessive water on acetaldehyde degradation due to the presence of competitive interactions between acetaldehyde and water. On the other hand, the decrease in the conversion is comparable to the decrease reported in literature [73]. Furthermore, the conversion in humid environment is still much higher (61%) than the conversion observed for commercial P25, even when tested in a relatively dry environment with a RH of 3–5 % (29 %). This difference highlights its potential for the application in indoor conditions.

4. Conclusion

In this study, mesoporous titania samples with appreciable surface area (30-90 m^2g^{-1}), preferentially exposed (001) facets, nanocrystals, and variable content of hydroxyl groups were prepared via a solvothermal method for highly efficient photocatalytic degradation of acetaldehyde. In particular, the impact of the interaction strength between the titania surface and surface water on the photocatalytic acetaldehyde degradation was explored. The correlation between the degradation performance and the physico-chemical properties of the samples was revealed.

As the solvothermal time increased at a constant temperature of 180 °C, the pore volume, surface area, and the content of surface OH groups overall increased while the crystal size overall decreased, which all have a positive impact on the acetaldehyde degradation efficiency. The obtained results showed that almost all samples displayed a similar or even better acetaldehyde degradation performance as compared with commercial P25. When the solvothermal temperature and time were 180 °C and 5 h, respectively, the prepared TiO_2 exhibited the most efficient performance, outperforming samples from literature even under harsher measurement conditions. The sample is characterized by an optimal set of parameters, including more porous structure, higher surface area and content of surface hydroxyl groups.

Additionally, it exhibits a weaker interaction strength between the titania surface and surface water, reducing competitive adsorption of surface water and acetaldehyde onto titania, thereby improving the acetaldehyde adsorption capacity thus providing an additional advantageous contribution to it superior performance. Moreover, the best-performing sample additionally showed a highly stable degradation performance, with no deactivation observed even after 48 h. Even when employed in a more realistic atmosphere at a RH of 30 %, the acetaldehyde degradation efficiency retains 82 % of its performance in a dry atmosphere (RH of 3-5 %), still strongly outperforming P25. This indicates its potential in practical applications such as indoor air cleaning. Finally, the findings from this study can now also be translated to photocatalytic degradation applications for other VOCs which have similar chemical properties, such as being easily soluble in water, providing a contribution with extended significance in the field of air pollution control.

Funding Source

J.W acknowledges the State Scholarship funded by the China Scholarship Council (201806060123). R.N. and S.V. acknowledge the University of Antwerp for financial support (GOA).

Note

The authors declare no competing financial interest.

CRediT authorship contribution statement

Kaimin Zhang: Conceptualization, Methodology, Validation, Investigation, Writing-original draft, Visualization. **Jinxin Wang**: Conceptualization, Methodology, Validation, Investigation, Visualization, Writing-review & editing. **Rajeshreddy Ninakanti**: Investigation, Visualization, Writing-review & editing. **Sammy W. Verbruggen**: Supervision, Methodology, Resources, Writing-review & editing.

References

[1] T. Salthammer, F. Fuhrmann, Photocatalytic surface reactions on indoor wall paint, Environ. Sci. Technol. 41 (2007) 6573–6578. https://doi.org/10.1021/es070057m.

[2] F. Shiraishi, M. Iwanaga, N. Kitagawa, F. Miyazaki, Enhancing the photocatalytic decomposition of acetaldehyde in air by immobilized titanium dioxide, J. Chem. Technol. Biotechnol. 95 (2020) 2034–2044. https://doi.org/10.1002/jctb.6396.

[3] B. Tryba, S. Jafari, M. Sillanpää, A. Nitta, B. Ohtani, A.W. Morawski, Influence of TiO_2 structure on its photocatalytic activity towards acetaldehyde decomposition, Appl. Surf. Sci. 470 (2019) 376–385. https://doi.org/10.1016/j.apsusc.2018.11.137.

[4] Y. Hu, X. Xie, X. Wang, Y. Wang, Y. Zeng, D.Y.H. Pui, J. Sun, Visible-Light Upconversion Carbon Quantum Dots Decorated TiO_2 for the Photodegradation of Flowing Gaseous Acetaldehyde, Appl. Surf. Sci. 440 (2018) 266–274. https://doi.org/10.1016/j.apsusc.2018.01.104.

[5] P. Makoś-Chełstowska, VOCs absorption from gas streams using deep eutectic solvents – A review, J. Hazard. Mater. 448 (2023). https://doi.org/10.1016/j.jhazmat.2023.130957.

[6] X. Li, L. Zhang, Z. Yang, P. Wang, Y. Yan, J. Ran, Adsorption materials for volatile organic compounds (VOCs) and the key factors for VOCs adsorption process: A review, Sep. Purif. Technol. 235 (2020) 116213. https://doi.org/10.1016/j.seppur.2019.116213.

[7] X. Li, J. Ma, X. Ling, Design and dynamic behaviour investigation of a novel VOC recovery system based on a deep condensation process, Cryogenics (Guildf). 107 (2020) 103060. https://doi.org/10.1016/j.cryogenics.2020.103060.

[8] B. Hauchecorne, D. Terrens, S. Verbruggen, J.A. Martens, H. Van Langenhove, K. Demeestere, S. Lenaerts, Elucidating the photocatalytic degradation pathway of acetaldehyde: An FTIR in situ study under atmospheric conditions, Appl. Catal. B Environ. 106 (2011) 630–638. https://doi.org/10.1016/j.apcatb.2011.06.026.

[9] S. Wang, H.M. Ang, M.O. Tade, Volatile organic compounds in indoor environment and photocatalytic oxidation: State of the art, Environ. Int. 33 (2007) 694–705. https://doi.org/10.1016/j.envint.2007.02.011.

[10] L. Zhong, J.J. Brancho, S. Batterman, B.M. Bartlett, C. Godwin, Experimental and modeling study of visible light responsive photocatalytic oxidation (PCO) materials for toluene degradation, Appl. Catal. B Environ. 216 (2017) 122–132. https://doi.org/10.1016/j.apcatb.2017.05.047.

[11] M.N. Lyulyukin, P.A. Kolinko, D.S. Selishchev, D. V. Kozlov, Hygienic aspects of TiO_2-mediated photocatalytic oxidation of volatile organic compounds: Air purification analysis using a total hazard index, Appl. Catal. B Environ. 220 (2018) 386–396. https://doi.org/10.1016/j.apcatb.2017.08.020.

[12] Y. Boyjoo, H. Sun, J. Liu, V.K. Pareek, S. Wang, A review on photocatalysis for air treatment: From catalyst development to reactor design, Chem. Eng. J. 310 (2017) 537–559. https://doi.org/10.1016/j.cej.2016.06.090.

[13] S.W. Verbruggen, TiO_2 photocatalysis for the degradation of pollutants in gas phase: From morphological design to plasmonic enhancement, J. Photochem. Photobiol. C Photochem. Rev. 24 (2015) 64–82. https://doi.org/10.1016/j.jphotochemrev.2015.07.001.

[14] R. deRichter, S. Caillol, Fighting global warming: The potential of photocatalysis against CO_2, CH_4, N_2O, CFCs, tropospheric O_3, BC and other major contributors to climate change, J. Photochem. Photobiol. C Photochem. Rev. 12 (2011) 1–19. https://doi.org/10.1016/j.jphotochemrev.2011.05.002.

[15] M. Van Hal, S.W. Verbruggen, X.Y. Yang, S. Lenaerts, T. Tytgat, Image analysis and in situ

FTIR as complementary detection tools for photocatalytic soot oxidation, Chem. Eng. J. 367 (2019) 269–277. https://doi.org/10.1016/j.cej.2019.02.154.

[16] S.W. Verbruggen, S. Deng, M. Kurttepeli, D.J. Cott, P.M. Vereecken, S. Bals, J.A. Martens, C. Detavernier, S. Lenaerts, Photocatalytic acetaldehyde oxidation in air using spacious TiO_2 films prepared by atomic layer deposition on supported carbonaceous sacrificial templates, Appl. Catal. B Environ. 160–161 (2014) 204–210. https://doi.org/10.1016/j.apcatb.2014.05.029.

[17] J. Low, B. Cheng, J. Yu, Surface modification and enhanced photocatalytic CO_2 reduction performance of TiO_2 : a review, Appl. Surf. Sci. 392 (2017) 658–686. https://doi.org/10.1016/j.apsusc.2016.09.093.

[18] I. Troppová, M. Šihor, M. Reli, M. Ritz, P. Praus, K. Kočí, Unconventionally prepared TiO_2/g-C_3N_4 photocatalysts for photocatalytic decomposition of nitrous oxide, Appl. Surf. Sci. 430 (2018) 335–347. https://doi.org/10.1016/j.apsusc.2017.06.299.

[19] L. Obalová, M. Reli, J. Lang, V. Matějka, J. Kukutschová, Z. Lacný, K. Kočí, Photocatalytic decomposition of nitrous oxide using TiO_2 and Ag-TiO_2 nanocomposite thin films, Catal. Today. 209 (2013) 170–175. https://doi.org/10.1016/j.cattod.2012.11.012.

[20] N. Blommaerts, R. Asapu, N. Claes, S. Bals, S. Lenaerts, S.W. Verbruggen, Gas phase photocatalytic spiral reactor for fast and efficient pollutant degradation, Chem. Eng. J. 316 (2017) 850–856. https://doi.org/10.1016/j.cej.2017.02.038.

[21] E. Pargoletti, L. Rimoldi, D. Meroni, G. Cappelletti, Photocatalytic removal of gaseous ethanol, acetaldehyde and acetic acid: from a fundamental approach to real cases, Int. Mater. Rev. 67 (2022) 864–897. https://doi.org/10.1080/09506608.2021.2017390.

[22] Y. Matsukawa, S. Hirata, M. Inada, N. Enomoto, J. Hojo, K. Hayashi, Kinetic effects of polymorphs and surface areas on adsorption and photocatalytic decomposition of acetaldehyde on titania, Chem. Eng. J. 397 (2020) 125422. https://doi.org/10.1016/j.cej.2020.125422.

[23] J. Ni, W. Wang, D. Liu, Q. Zhu, J. Jia, J. Tian, Z. Li, X. Wang, Z. Xing, Oxygen vacancy-mediated sandwich-structural TiO_{2-x} /ultrathin g-C_3N_4/TiO_{2-x} direct Z-scheme heterojunction visible-light-driven photocatalyst for efficient removal of high toxic tetracycline antibiotics, J. Hazard. Mater. 408 (2021). https://doi.org/10.1016/j.jhazmat.2020.124432.

[24] K. Yaemsunthorn, M. Kobielusz, W. Macyk, TiO_2 with Tunable Anatase-to-Rutile Nanoparticles Ratios: How Does the Photoactivity Depend on the Phase Composition and the Nature of Photocatalytic Reaction?, ACS Appl. Nano Mater. 4 (2021) 633–643. https://doi.org/10.1021/acsanm.0c02932.

[25] H. Zong, T. Zhao, G. Zhou, R. Qian, T. Feng, J.H. Pan, Revisiting structural and photocatalytic properties of g-C_3N_4/TiO_2: Is surface modification of TiO_2 by calcination with urea an effective route to “solar” photocatalyst?, Catal. Today. 335 (2019) 252–261. https://doi.org/10.1016/j.cattod.2018.12.015.

[26] S. Deng, S.W. Verbruggen, Z. He, D.J. Cott, P.M. Vereecken, J.A. Martens, S. Bals, S. Lenaerts, C. Detavernier, Atomic layer deposition-based synthesis of photoactive TiO_2 nanoparticle chains by using carbon nanotubes as sacrificial templates, RSC Adv. 4 (2014) 11648–11653. https://doi.org/10.1039/c3ra42928h.

[27] S.W. Verbruggen, K. Masschaele, E. Moortgat, T.E. Korany, B. Hauchecorne, J.A. Martens, S. Lenaerts, Factors driving the activity of commercial titanium dioxide powders towards gas phase photocatalytic oxidation of acetaldehyde, Catal. Sci. Technol. 2 (2012) 2311–2318. https://doi.org/10.1039/c2cy20123b.

[28] J. Lyu, L. Zhou, J. Shao, Z. Zhou, J. Gao, J. Li, Y. Dong, Z. Wang, Synthesis of TiO_2/$H_2Ti_3O_7$

composite with nanoscale spiny hollow hierarchical structure for photocatalytic mineralization of VOCs, Chem. Eng. J. 400 (2020) 125927. https://doi.org/10.1016/j.cej.2020.125927.

[29] G. He, J. Zhang, Y. Hu, Z. Bai, C. Wei, Dual-template synthesis of mesoporous TiO_2 nanotubes with structure-enhanced functional photocatalytic performance, Appl. Catal. B Environ. 250 (2019) 301–312. https://doi.org/10.1016/j.apcatb.2019.03.027.

[30] C.L. Bianchi, S. Gatto, C. Pirola, A. Naldoni, A. Di Michele, G. Cerrato, V. Crocellà, V. Capucci, Photocatalytic degradation of acetone, acetaldehyde and toluene in gas-phase: Comparison between nano and micro-sized TiO_2, Appl. Catal. B Environ. 146 (2014) 123–130. https://doi.org/10.1016/j.apcatb.2013.02.047.

[31] G. Zhang, Y. Liu, Z. Hashisho, Z. Sun, S. Zheng, L. Zhong, Adsorption and photocatalytic degradation performances of TiO_2/diatomite composite for volatile organic compounds: Effects of key parameters, Appl. Surf. Sci. 525 (2020) 146633. https://doi.org/10.1016/j.apsusc.2020.146633.

[32] B.I. Stefanov, G.A. Niklasson, C.G. Granqvist, L. Österlund, Gas-phase photocatalytic activity of sputter-deposited anatase TiO_2 films: Effect of (001) preferential orientation, surface temperature and humidity, J. Catal. 335 (2016) 187–196. https://doi.org/10.1016/j.jcat.2015.12.002.

[33] J. Zhang, K. Vikrant, K.H. Kim, F. Dong, M. Won Chung, S. Weon, Unveiling the collective effects of moisture and oxygen on the photocatalytic degradation of m-Xylene using a titanium dioxide supported platinum catalyst, Chem. Eng. J. 439 (2022) 135747. https://doi.org/10.1016/j.cej.2022.135747.

[34] K. Demeestere, J. Dewulf, H. Van Langenhove, B. Sercu, Gas-solid adsorption of selected volatile organic compounds on titanium dioxide Degussa P25, Chem. Eng. Sci. 58 (2003) 2255–2267. https://doi.org/10.1016/S0009-2509(03)00087-3.

[35] I. Sopyan, Kinetic analysis on photocatalytic degradation of gaseous acetaldehyde, ammonia and hydrogen sulfide on nanosized porous TiO_2 films, Sci. Technol. Adv. Mater. 8 (2007) 33–39. https://doi.org/10.1016/j.stam.2006.10.004.

[36] B. Tryba, P. Rychtowski, A. Markowska-Szczupak, J. Przepiórski, Photocatalytic decomposition of acetaldehyde on different TiO_2-based materials: A review, Catalysts. 10 (2020) 1–26. https://doi.org/10.3390/catal10121464.

[37] A. Chakraborty, Samriti, O. Ruzimuradov, R.K. Gupta, J. Cho, J. Prakash, TiO_2 nanoflower photocatalysts: Synthesis, modifications and applications in wastewater treatment for removal of emerging organic pollutants, Environ. Res. 212 (2022) 113550. https://doi.org/10.1016/j.envres.2022.113550.

[38] A.H. Mamaghani, F. Haghighat, C.-S. Lee, Hydrothermal/solvothermal synthesis and treatment of TiO_2 for photocatalytic degradation of air pollutants: Preparation, characterization, properties, and performance, Chemosphere. 219 (2019) 804–825. https://doi.org/10.1016/j.chemosphere.2018.12.029.

[39] C. Wang, X. Zhang, Y. Liu, Coexistence of an anatase/TiO_2(B) heterojunction and an exposed (001) facet in TiO_2 nanoribbon photocatalysts synthesized via a fluorine-free route and topotactic transformation, Nanoscale. 6 (2014) 5329–5337. https://doi.org/10.1039/c4nr00236a.

[40] K. Lan, R. Wang, W. Zhang, Z. Zhao, A. Elzatahry, X. Zhang, Y. Liu, D. Al-Dhayan, Y. Xia, D. Zhao, Mesoporous TiO_2 Microspheres with Precisely Controlled Crystallites and Architectures, Chem. 4 (2018) 2436–2450. https://doi.org/10.1016/j.chempr.2018.08.008.

[41] G.T.S. How, A. Pandikumar, H.N. Ming, L.H. Ngee, Highly exposed {001} facets of titanium

dioxide modified with reduced graphene oxide for dopamine sensing, Sci. Rep. 4 (2014) 2–9. https://doi.org/10.1038/srep05044.

[42] M. Van Hal, R. Campos, S. Lenaerts, K. De Wael, S.W. Verbruggen, Gas phase photofuel cell consisting of WO_3- and TiO_2-photoanodes and an air-exposed cathode for simultaneous air purification and electricity generation, Appl. Catal. B Environ. 292 (2021) 120204. https://doi.org/10.1016/j.apcatb.2021.120204.

[43] R. Asapu, N. Claes, S. Bals, S. Denys, C. Detavernier, S. Lenaerts, S.W. Verbruggen, Silver-polymer core-shell nanoparticles for ultrastable plasmon-enhanced photocatalysis, Appl. Catal. B Environ. 200 (2017) 31–38. https://doi.org/10.1016/j.apcatb.2016.06.062.

[44] M. Thommes, K. Kaneko, A. V. Neimark, J.P. Olivier, F. Rodriguez-Reinoso, J. Rouquerol, K.S.W. Sing, Physisorption of gases, with special reference to the evaluation of surface area and pore size distribution (IUPAC Technical Report), Pure Appl. Chem. 87 (2015) 1051–1069. https://doi.org/10.1515/pac-2014-1117.

[45] A.K. Datye, G. Riegel, J.R. Bolton, M. Huang, M.R. Prairie, Microstructural characterization of a fumed titanium dioxide photocatalyst, J. Solid State Chem. 115 (1995) 236–239. https://doi.org/10.1006/jssc.1995.1126.

[46] K. Li, Z. Huang, X. Zeng, B. Huang, S. Gao, J. Lu, Synergetic Effect of Ti_3^+ and Oxygen Doping on Enhancing Photoelectrochemical and Photocatalytic Properties of TiO_2/g-C_3N_4 Heterojunctions, ACS Appl. Mater. Interfaces. 9 (2017) 11577–11586. https://doi.org/10.1021/acsami.6b16191.

[47] Y.R. Lv, C.J. Liu, R.K. He, X. Li, Y.H. Xu, $BiVO_4$/TiO_2 heterojunction with enhanced photocatalytic activities and photoelectochemistry performances under visible light illumination, Mater. Res. Bull. 117 (2019) 35–40. https://doi.org/10.1016/j.materresbull.2019.04.032.

[48] A.L. Patterson, The Scherrer Formula for X-Ray Particle Size Determination, Phys. Rev. 56 (1939) 978–982. https://doi.org/10.1103/PhysRev.56.978.

[49] S. Velázquez-Martínez, S. Silva-Martínez, A.E. Jiménez-González, A. Maldonado Álvarez, Synthesis of Mesoporous TiO_2 Spheres via the Solvothermal Process and Its Application in the Development of DSSC, Adv. Mater. Sci. Eng. 2019 (2019). https://doi.org/10.1155/2019/9504198.

[50] Y.C. Zhang, M. Yang, G. Zhang, D.D. Dionysiou, HNO_3-involved one-step low temperature solvothermal synthesis of N-doped TiO_2 nanocrystals for efficient photocatalytic reduction of Cr(VI) in water, Appl. Catal. B Environ. 142–143 (2013) 249–258. https://doi.org/10.1016/j.apcatb.2013.05.023.

[51] C. Su, C.M. Tseng, L.F. Chen, B.H. You, B.C. Hsu, S.S. Chen, Sol-hydrothermal preparation and photocatalysis of titanium dioxide, Thin Solid Films. 498 (2006) 259–265. https://doi.org/10.1016/j.tsf.2005.07.123.

[52] F. Batault, F. Thevenet, V. Hequet, C. Rillard, L. Le Coq, N. Locoge, Acetaldehyde and acetic acid adsorption on TiO_2 under dry and humid conditions, Chem. Eng. J. 264 (2015) 197–210. https://doi.org/10.1016/j.cej.2014.10.089.

[53] C. Wang, Z. Rao, A. Mahmood, X. Wang, Y. Wang, X. Xie, J. Sun, Improved photocatalytic oxidation performance of gaseous acetaldehyde by ternary g-C_3N_4/Ag-TiO_2 composites under visible light, J. Colloid Interface Sci. 602 (2021) 699–711. https://doi.org/10.1016/j.jcis.2021.05.186.

[54] J.G. Van Dijck, H. Lenaerts, L. Siemons, F. Blockhuys, V. Meynen, The interaction of water with organophosphonic acid surface modified titania: An in-depth in-situ DRIFT study,

Surfaces and Interfaces. 21 (2020) 100710. https://doi.org/10.1016/j.surfin.2020.100710.

[55] R. Mueller, H.K. Kammler, K. Wegner, S.E. Pratsinis, OH surface density of SiO_2 and TiO_2 by thermogravimetric analysis, Langmuir. 19 (2003) 160–165. https://doi.org/10.1021/la025785w.

[56] A. Di Paola, M. Bellardita, L. Palmisano, Z. Barbieriková, V. Brezová, Influence of crystallinity and OH surface density on the photocatalytic activity of TiO_2 powders, J. Photochem. Photobiol. A Chem. 273 (2014) 59–67. https://doi.org/10.1016/j.jphotochem.2013.09.008.

[57] J. Zhu, S. Wang, Z. Bian, S. Xie, C. Cai, J. Wang, H. Yang, H. Li, Solvothermally controllable synthesis of anatase TiO_2 nanocrystals with dominant {001} facets and enhanced photocatalytic activity, CrystEngComm. 12 (2010) 2219–2224. https://doi.org/10.1039/C000128G.

[58] A.C.C. Alves Melo, R.A. de Jesus, A.C. de M. Olivera, G.R. Salazar-Banda, H.M.C. Andrade, R.M.N. Yerga, J.L.G. Fierro, M. Bilal, H.M.N. Iqbal, L.F.R. Ferreira, R.T. Figueiredo, Effect of non-ionic surfactant in the solvothermal synthesis of anatase TiO_2 nanoplates with a high percentage of exposed {001} facets and its role in the photocatalytic degradation of methylene blue dye, Environ. Res. 214 (2022). https://doi.org/10.1016/j.envres.2022.114094.

[59] H.G. Yang, G. Liu, S.Z. Qiao, C.H. Sun, Y.G. Jin, S.C. Smith, J. Zou, H.M. Cheng, G.Q. (Max) Lu, Solvothermal Synthesis and Photoreactivity of Anatase TiO_2 Nanosheets with Dominant {001} Facets, J. Am. Chem. Soc. 131 (2009) 4078–4083. https://doi.org/10.1021/ja808790p.

[60] J.S. Chen, Y.L. Tan, C.M. Li, Y.L. Cheah, D. Luan, S. Madhavi, F.Y.C. Boey, L.A. Archer, X.W. Lou, Constructing hierarchical spheres from large ultrathin anatase TiO_2 nanosheets with nearly 100% exposed (001) facets for fast reversible lithium storage, J. Am. Chem. Soc. 132 (2010) 6124–6130. https://doi.org/10.1021/ja100102y.

[61] Y. Mao, S. Mao, Z.G. Ye, Z. Xie, L. Zheng, Solvothermal synthesis and Curie temperature of monodispersed barium titanate nanoparticles, Mater. Chem. Phys. 124 (2010) 1232–1238. https://doi.org/10.1016/j.matchemphys.2010.08.063.

[62] X. Wang, G. Liu, L. Wang, J. Pan, G.Q. Lu, H.M. Cheng, TiO_2 films with oriented anatase {001} facets and their photoelectrochemical behavior as CdS nanoparticle sensitized photoanodes, J. Mater. Chem. 21 (2011) 869–873. https://doi.org/10.1039/c0jm02694h.

[63] M.M. Maitani, A. Tateyama, P.P. Boix, G. Han, A. Nitta, B. Ohtani, N. Mathews, Y. Wada, Effects of energetics with {001} facet-dominant anatase TiO_2 scaffold on electron transport in CH3NH3PbI3 perovskite solar cells, Electrochim. Acta. 300 (2019) 445–454. https://doi.org/10.1016/j.electacta.2019.01.102.

[64] F. Pellegrino, F. Sordello, L. Mino, C. Minero, V.-D. Hodoroaba, G. Martra, V. Maurino, Formic Acid Photoreforming for Hydrogen Production on Shape-Controlled Anatase TiO_2 Nanoparticles: Assessment of the Role of Fluorides, {101}/{001} Surfaces Ratio, and Platinization, ACS Catal. 9 (2019) 6692–6697. https://doi.org/10.1021/acscatal.9b01861.

[65] R. Liu, F. Yang, Y. Xie, Y. Yu, Visible-light responsive boron and nitrogen codoped anatase TiO_2 with exposed {001} facet: Calculation and experiment, Appl. Surf. Sci. 466 (2019) 568–577. https://doi.org/10.1016/j.apsusc.2018.10.058.

[66] M. Strauss, M. Pastorello, F.A. Sigoli, J.M. De Souza E Silva, I.O. Mazali, Singular effect of crystallite size on the charge carrier generation andphotocatalytic activity of nano-TiO_2, Appl. Surf. Sci. 319 (2014) 151–157. https://doi.org/10.1016/j.apsusc.2014.06.071.

[67] D.S. Kim, S.J. Han, S.Y. Kwak, Synthesis and photocatalytic activity of mesoporous TiO_2

with the surface area, crystallite size, and pore size, J. Colloid Interface Sci. 316 (2007) 85–91. https://doi.org/10.1016/j.jcis.2007.07.037.

[68] Z. Gao, J. Wang, Y. Muhammad, Y. Zhang, S.J. Shah, Y. Hu, Z. Chu, Z. Zhao, Z. Zhao, Enhanced moisture-resistance and excellent photocatalytic performance of synchronous N/Zn-decorated MIL-125(Ti) for vaporous acetaldehyde degradation, Chem. Eng. J. 388 (2020) 124389. https://doi.org/10.1016/j.cej.2020.124389.

[69] Z. Rao, G. Shi, Z. Wang, A. Mahmood, X. Xie, J. Sun, Photocatalytic degradation of gaseous VOCs over Tm^{3+}-TiO_2: Revealing the activity enhancement mechanism and different reaction paths, Chem. Eng. J. 395 (2020) 125078. https://doi.org/10.1016/j.cej.2020.125078.

[70] B. Tryba, P. Rychtowski, J. Srenscek-Nazzal, J. Przepiorski, The inflence of TiO_2 structure on the complete decomposition of acetaldehyde gas, Mater. Res. Bull. 126 (2020). https://doi.org/10.1016/j.materresbull.2020.110816.

[71] Q. Zeng, X. Wang, X. Xie, A. Mahmood, G. Lu, Y. Wang, J. Sun, Band bending of TiO_2 induced by O-xylene and acetaldehyde adsorption and its effect on the generation of active radicals, J. Colloid Interface Sci. 572 (2020) 374–383. https://doi.org/10.1016/j.jcis.2020.03.114.

[72] A. Mahmood, G. Shi, X. Xie, J. Sun, Assessing the adsorption and photocatalytic activity of TiO_2 nanoparticles for the gas phase acetaldehyde: A computational and experimental study, J. Alloys Compd. 819 (2020) 153055. https://doi.org/10.1016/j.jallcom.2019.153055.

[73] S. Zhao, Y. Ji, M. Jeong, H. Choe, J.W. Lee, S.Y. Kim, S. Saqlain, Z. Peng, Z. Liu, Y.D. Kim, Enhanced photocatalytic activity of TiO2 by K incorporation towards acetaldehyde and NO oxidation: The role of K single-ion dopants and additional K-compound structures, Chem. Eng. J. 444 (2022) 136500. https://doi.org/10.1016/j.cej.2022.136500.